



ALMA MATER STUDIORUM
UNIVERSITÀ DI BOLOGNA

ARCHIVIO ISTITUZIONALE
DELLA RICERCA

Alma Mater Studiorum Università di Bologna Archivio istituzionale della ricerca

A late Neanderthal tooth from northeastern Italy

This is the final peer-reviewed author's accepted manuscript (postprint) of the following publication:

Published Version:

A late Neanderthal tooth from northeastern Italy / Romandini M.; Oxilia G.; Bortolini E.; Peyregne S.; Delpiano D.; Nava A.; Panetta D.; Di Domenico G.; Martini P.; Arrighi S.; Badino F.; Figus C.; Lugli F.; Marciani G.; Silvestrini S.; Menghi Sartorio J.C.; Terlato G.; Hublin J.-J.; Meyer M.; Bondioli L.; Higham T.; Slon V.; Peresani M.; Benazzi S.. - In: JOURNAL OF HUMAN EVOLUTION. - ISSN 0047-2484. - ELETTRONICO. - 147:(2020), pp. 102867.1-102867.13. [10.1016/j.jhevol.2020.102867]

Availability:

This version is available at: <https://hdl.handle.net/11585/773013> since: 2020-09-29

Published:

DOI: <http://doi.org/10.1016/j.jhevol.2020.102867>

Terms of use:

Some rights reserved. The terms and conditions for the reuse of this version of the manuscript are specified in the publishing policy. For all terms of use and more information see the publisher's website.

This item was downloaded from IRIS Università di Bologna (<https://cris.unibo.it/>).
When citing, please refer to the published version.

(Article begins on next page)

This is the final peer-reviewed accepted manuscript of:

M. Romandini, G. Oxilia, E. Bortolini, S. Peyrégne, D. Delpiano, A. Nava, D. Panetta, G. Di Domenico, P. Martini, S. Arrighi, F. Badino, C. Figus, F. Lugli, G. Marciani, S. Silvestrini, J. C. Menghi Sartorio, G. Terlato, J.J. Hublin, M. Meyer, L. Bondioli, T. Higham, V. Slon, M. Peresani, S. Benazzi, A late Neanderthal tooth from northeastern Italy, *Journal of Human Evolution*, 147 (2020), 102867

The final published version is available online at:

<https://doi.org/10.1016/j.jhevol.2020.102867>

Rights / License:

The terms and conditions for the reuse of this version of the manuscript are specified in the publishing policy. For all terms of use and more information see the publisher's website.

This item was downloaded from IRIS Università di Bologna (<https://cris.unibo.it/>)

When citing, please refer to the published version.

A late Neanderthal tooth from northeastern Italy

Matteo Romandini ^{a,*}, Gregorio Oxilia ^{a,1}, Eugenio Bortolini ^{a,1}, Stéphane Peyrégne ^b, Davide Delpiano ^c, Alessia Nava ^{d,e}, Daniele Panetta ^f, Giovanni Di Domenico ^g, Petra Martini ^h, Simona Arrighi ^a, Federica Badino ^{a,i}, Carla Figus ^a, Federico Lugli ^a, Giulia Marciani ^a, Sara Silvestrini ^a, Jessica C. Menghi Sartorio ^c, Gabriele Terlato ^c, Jean-Jacques Hublin ^{j,k}, Matthias Meyer ^b, Luca Bondioli ^e, Thomas Higham ^l, Viviane Slon ^b, Marco Peresani ^{c,§}, Stefano Benazzi ^{a,j,§}

^a *Department of Cultural Heritage, University of Bologna, Via degli Ariani 1, 48121, Ravenna, Italy*

^b *Department of Evolutionary Genetics, Max Planck Institute for Evolutionary Anthropology, Deutscher Platz 6, Leipzig 04103, Germany*

^c *Università di Ferrara, Dipartimento di Studi Umanistici, Sezione di Scienze Preistoriche e Antropologiche, Corso Ercole I d'Este 32, 44100, Ferrara, Italy*

^d *DANTE Laboratory for the study of Diet and Ancient Technology, Sapienza University of Rome, Rome, Italy*

^e *Bioarchaeology Service, Museo delle Civiltà, Rome, Italy*

^f *CNR Institute of Clinical Physiology, National Research Council, Via G. Moruzzi 1, 56124 Pisa, Italy*

^g *Università di Ferrara, Dipartimento di Fisica e Scienze della Terra, Via Saragat 1, 44122, Ferrara, Italy*

^h *Department of Morphology, Surgery and Experimental Medicine, University of Ferrara, Via Luigi Borsari, 46-44121 Ferrara, Italy*

ⁱ *C.N.R, Istituto di Geologia Ambientale e Geoingegneria, 20126, Milano, Italy*

This item was downloaded from IRIS Università di Bologna (<https://cris.unibo.it/>)

When citing, please refer to the published version.

^j *Department of Human Evolution, Max Planck Institute for Evolutionary Anthropology, Deutscher Platz 6, Leipzig 04103, Germany*

^k *Collège de France, Place Marcellin Berthelot 11, 75005 Paris, France*

^l *Oxford Radiocarbon Accelerator Unit Research Lab for Archaeology and the History of Art
University of Oxford OX1 3TG, UK*

*Corresponding author.

E-mail address: matteo.romandini@unibo.it (M. Romandini).

¹ These authors contributed equally to this work. [§]Senior authors

This item was downloaded from IRIS Università di Bologna (<https://cris.unibo.it/>)

When citing, please refer to the published version.

Abstract

The site of Riparo Broion (Vicenza, northeastern Italy) preserves a stratigraphic sequence documenting the Middle to Upper Paleolithic transition, in particular the final Mousterian and the Uluzzian cultures. In 2018 a human tooth was retrieved from a late Mousterian level, representing the first human remain ever found from this rock shelter (Riparo Broion 1). Here we provide the morphological description and taxonomic assessment of Riparo Broion 1 with the support of classic and virtual morphology, 2D and 3D analysis of the topography of enamel thickness, and DNA analysis. The tooth is an exfoliated right upper deciduous canine, and its general morphology and enamel thickness distribution support attribution to a Neanderthal child. Correspondingly, the mitochondrial DNA sequence from Riparo Broion 1 falls within the known genetic variation of Late Pleistocene Neanderthals, in accordance with newly obtained radiocarbon dates which point to approximately 48 ka cal BP as the most likely minimum age for this specimen. The present work describes novel and direct evidence of the late Neanderthal occupation in northern Italy that preceded the marked cultural and technological shift documented by the Uluzzian layers in the archaeological sequence at Riparo Broion. Here we provide a new full morphological, morphometric, and taxonomic analysis of Riparo Broion 1, in addition to generating the wider reference sample of Neanderthal and modern human upper deciduous canines. This research contributes to increasing the sample of fossil remains from Italy, as well as the number of currently available upper deciduous canines, which are presently poorly documented in the scientific literature.

Keywords: Neanderthal; Deciduous human canine; Late Middle Paleolithic; Mediterranean Europe; Virtual analysis; 2D and 3D enamel thickness

This item was downloaded from IRIS Università di Bologna (<https://cris.unibo.it/>)

When citing, please refer to the published version.

1. Introduction

Our understanding of the biocultural processes underlying the arrival of modern humans in Europe, their potential interaction with Neanderthals, and the demise of the latter around 40 ka (Higham et al., 2014) is undermined by the inhomogeneous distribution of human remains dating to the Middle to Upper Paleolithic transition (Benazzi, 2012; Hublin, 2015).

Pertaining to this chronological horizon, only a handful of Neanderthal and modern human remains have been found in Italy in contexts dated to Marine Isotope Stage (MIS) 3 (~60–30 ka), the majority of which fall between 45–40 ka cal BP (Benazzi et al., 2018). The earliest examples include the Neanderthal teeth from Grotta di Fumane, found in layers A11 and A9 (with a minimum age of 47.6 ka cal BP; Benazzi et al., 2014b), and the undated Neanderthal teeth from level 36 at Riparo Tagliente (Arnaud et al., 2016). The more recent ones (~45–40 ka) include: the Neanderthal right dI₁ from Grotta del Cavallo (Cavallo D), dated to ~45 ka cal BP (Fabbri et al., 2016); two modern human deciduous premolars (Cavallo B, left dP³, and Cavallo C, left dP⁴) from the Uluzzian levels of the same cave (Benazzi et al., 2011a); two modern human deciduous teeth from the Protoaurignacian contexts of Riparo Bombrini (left dI₂) and Grotta di Fumane (Fumane 2, right dI²), dated to ~41–40 ka cal BP (Benazzi et al., 2015); and a taxonomically undiagnostic molar fragment from an uncertain context in layer A3 of Grotta di Fumane, i.e., Fumane 6 (Benazzi et al., 2014b).

The Italian human fossil record (Benazzi, 2018) and a recent reassessment of the stratigraphic sequence of Grotta del Cavallo (Moroni et al., 2018; Zanchetta et al., 2018) suggest that modern humans currently interpreted as associated with the Uluzzian industry were already present in southern Europe at least since 45 ka cal BP. However, modern humans potentially arrived in Europe even earlier, based on OSL dates (48.2 ± 1.9 ka; Richter et al., 2009) obtained for the Central European Upper Paleolithic Bohunician industry, which shows similarities with the Levantine Emirian (Skrdla, 2003; Tostevin, 2003; Bar-Yosef, 2003, 2007; Hoffecker, 2009) and on radiocarbon

This item was downloaded from IRIS Università di Bologna (<https://cris.unibo.it/>)

When citing, please refer to the published version.

dates (47–43 ka; Fewlass et al., 2020) obtained for the Upper Paleolithic industry found at Bacho Kiro (Bulgaria; Hublin et al., 2020). Therefore, based on available data, the period between 50–46 ka cal BP might be of critical importance to unravel the biocultural interactions between autochthonous Neanderthals and incoming modern humans.

Riparo Broion (Vicenza, Italy) is a key site whose archaeological sequence clearly documents the Middle to Early Upper Paleolithic transition (Peresani et al., 2019). The Mousterian layers—currently under study—lie immediately below the layers that possibly document the arrival of modern humans in the region and offer detailed evidence on subsistence strategies and material culture of the late Neanderthals that occupied the area. Like Grotta del Cavallo and Grotta di Fumane, Riparo Broion is one of the few archaeological sites in Italy with a complete stratigraphy involving Uluzzian occupation that yielded human fossils associated with late Middle Paleolithic remains.

In this study we provide a taxonomic attribution for Riparo Broion 1, hereafter called RB1, an exfoliated deciduous human canine found in 2018 in the Late Mousterian layer 11-lower at Riparo Broion. Taxonomic identification was determined by performing a morphological description, 2D and 3D analysis of the topography of enamel thickness, and mitochondrial DNA (mtDNA) analysis. Moreover, for the purpose of this study, we generated a comprehensive reference sample for upper deciduous human canines. Finally, to ascertain the relevance of this specimen for the critical period 50–46 ka cal BP, we radiocarbon dated the context of the finding and compared the results with other dates from the Mousterian and Uluzzian layers of the same site.

1.1. Archaeological and paleoenvironmental context

Riparo Broion is located on the eastern slope of the Berici Hills, at 135 m a.s.l. up a steep cliff face that connects the peak of Mount Brosimo (327 m a.s.l.) to the Friulian-Venetian plain (Fig. 1). The

This item was downloaded from IRIS Università di Bologna (<https://cris.unibo.it/>)

When citing, please refer to the published version.

rock shelter—which is 10 m long, 6 m deep and 17 m high—formed by a rock collapse along a major ENE–WSW oriented fault that developed because of thermoclastic processes and chemical dissolution (Sauro, 2002; Dal Lago and Mietto, 2003). Stratified deposits were dated to the Late Pleistocene and include evidence for the Middle/Upper Paleolithic transition. A detailed overview of the geographical and paleoecological setting, as well as of the archaeological excavation and sedimentary sequence uncovered at Riparo Broion, was recently published (Peresani et al., 2019).

Excavations spanning from 1998 to 2018 lead archaeologists to identify 11 stratigraphic units. Unit 1 was split into seven subunits (layers), from 1a to 1g. It shows the following cultural sequence: Early Epigravettian (layers 1a-1b); Gravettian (1c-1d); Uluzzian (1e-1f-1g); and Mousterian (units 4+7, 9 and 11). No evidence of anthropic activity has yet been documented in units 2 and 3. Recently, Peresani et al. (2019) argued the attribution of the lithic assemblage uncovered in the shelter to the Uluzzian, confirming the presence of this Early Upper Paleolithic culture in Northern Italy (Peresani, 2008; Peresani et al., 2016). In 2018, during excavation, a human tooth (Fig. 2) was uncovered in square AA3a in layer 11 top (Fig. 1).

This stratigraphic unit formed over a time interval that includes MIS 3 Greenland Interstadials (GI 14–12 (ca. 54.2–43.3 ka according to Rasmussen et al., 2014)—both characterized by large arboreal excursions (Fletcher et al., 2010). At this time, humid and mild conditions are registered in speleothem isotopic records from the eastern Mediterranean (Soreq cave; Bar-Matthews et al., 2000) and central Europe (Bunker Cave; Weber et al., 2018). The long GI14-12 interval is briefly interrupted by Greenland Stadial 13 (GS13, between 48.3 and 46.8 ka), which includes Heinrich event 5 (HE5), lasting about 1500 yr (Rasmussen et al., 2014). This shift brought severe aridity in the Mediterranean region (Fletcher and Sánchez Goñi et al., 2008; Fleitmann et al., 2009; Müller et al., 2011). In northeastern Italy, pollen data from Lake Fimon (Pini et al., 2010) and Azzano Decimo (Pini et al., 2009) point to a generally higher forest cover compared to Mediterranean sites. Indeed,

This item was downloaded from IRIS Università di Bologna (<https://cris.unibo.it/>)

When citing, please refer to the published version.

the glaciated Alps must have represented a very sharp rainfall boundary, leading to humid conditions in the southeastern Alpine foreland (Pini et al., 2010), as confirmed by micromammal associations examined at sites on the Berici Hills and Lessini Mountains (López-García et al., 2015, 2019).

Between ca. 55–45 ka, the paleoecological record of Fimon documents a number of phases of mixed conifer forest expansion with dominant *Pinus sylvestris-mugo* (mean value of ca. 38%, with peaks up to 70%), *Picea*, and cool broad-leaved trees (*Alnus* cf. *incana* and tree *Betula*). Temperate forest taxa (deciduous *Quercus* and other thermophilous taxa) contribute to 4% of the total record. Among these, *Tilia* persisted up to ca. 40 ka (Pini et al., 2010). Within the same interval, open environments—identified by pollen of herbaceous taxa (34%) and steppe/desert forb-shrubs (9%; i.e., *Artemisia* and Chenopodiaceae)—possibly expanded during GSs, with major vegetation changes during HEs (Allen et al., 1999; Tzedakis et al., 2006; Badino et al., 2019).

On a long-term scale, data suggest a dominant cool mixed forest biome, possibly consisting of open-forest formations of either boreal taxa or a mixture of boreal, eurythermic and temperate tree taxa. Such biome is expected to occur in climates with moderately cold winters (mean coldest-month temperatures from -2 to -15 °C), with enough growing degree days (GDD > 1200) for temperate summer-green trees, and enough precipitation (>75%) for boreal evergreen conifers (Prentice et al., 1992).

In this context, the preliminary analysis of zooarchaeological data uncovered in unit 11 at Riparo Broion shows the presence of a broad variety of species such as *Alces alces* (elk), *Cervus elaphus* (red deer), *Capreolus capreolus* (roe deer), *Megaloceros giganteus* (Irish elk/megaloceros), *Sus*

This item was downloaded from IRIS Università di Bologna (<https://cris.unibo.it/>)

When citing, please refer to the published version.

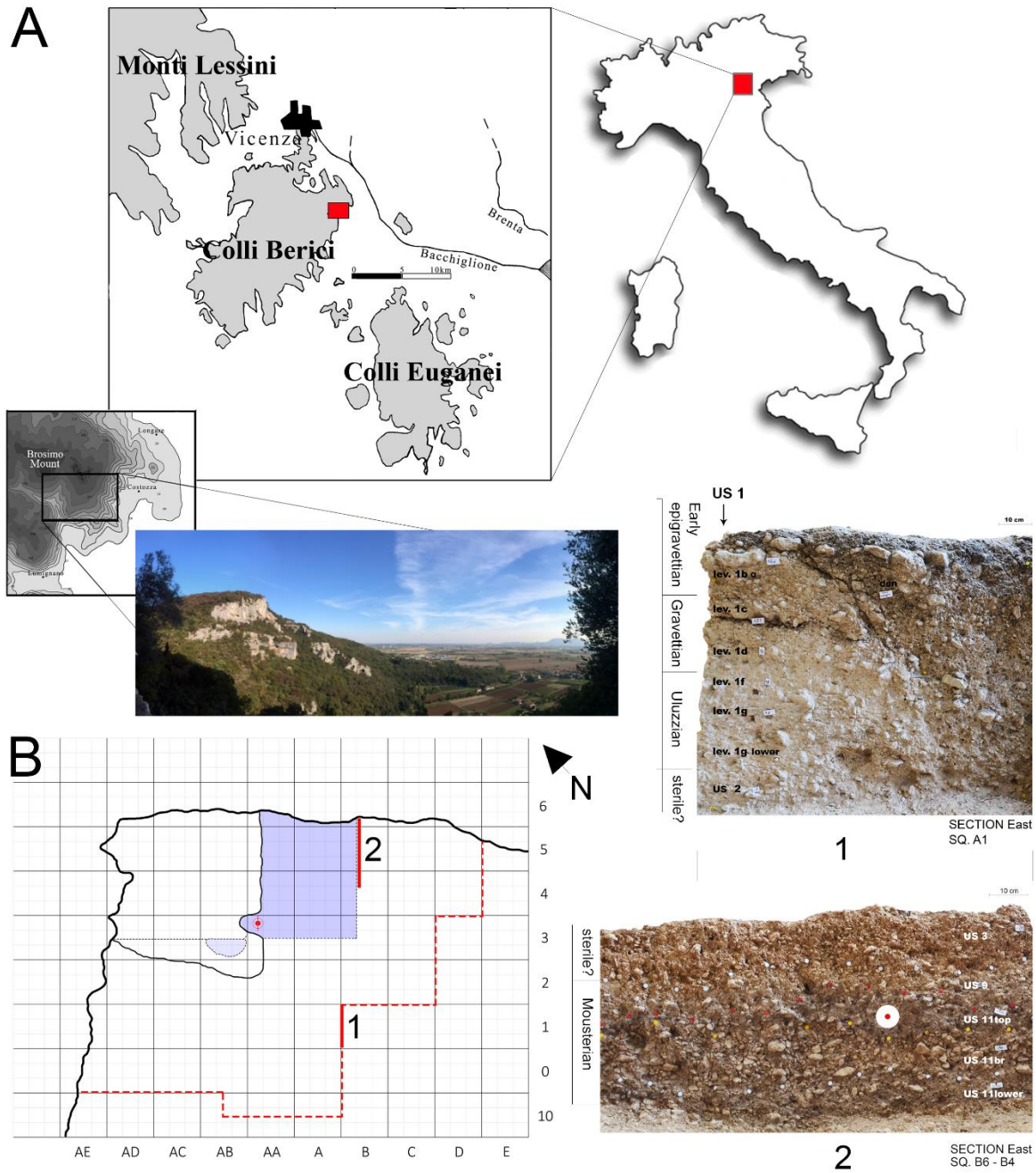


Figure 1. A) Geographic position of Riparo del Broion in the NE sector of the Berici Hills. B) General plan of the excavated area with position of unit 11 (blue area), the tooth (red circle), the section with the Upper Paleolithic sequence (1), the section with the Late Middle Paleolithic sequence (2), the extension of the excavated area (red dotted line).

This item was downloaded from IRIS Università di Bologna (<https://cris.unibo.it/>)

When citing, please refer to the published version.

scrofa (wild boar), *Bos primigenius* (aurochs) or *Bison priscus* (bison), a few goats and horses, and abundant *Castor fiber* (beaver) in association with scant remains of fish and freshwater bivalves (Unioniade). This assemblage supports the presence of environments ranging from open-spaced to dense and closed forests, with the addition of transitional and discontinuous Alpine grasslands or pioneer vegetation on carbonate rocks, completed by the presence of humid-marshy environments with weak water courses, wet meadows or shallow lakes.

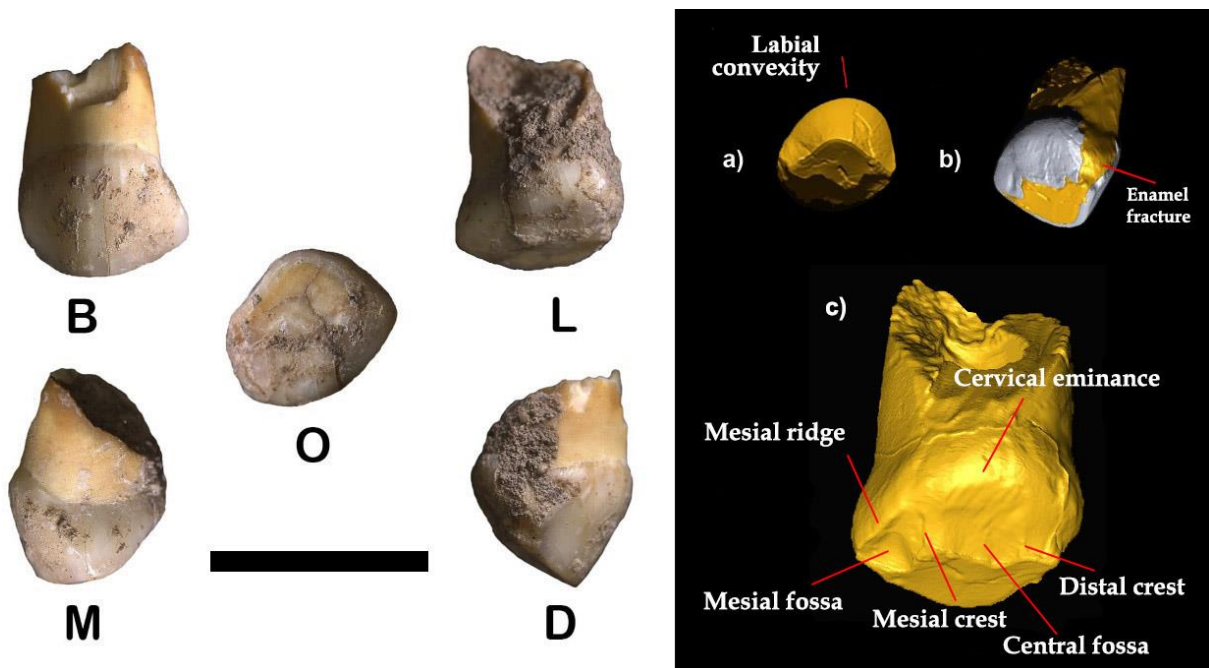


Figure 2. Riparo Broion 1 (RB1), right dC1, in different views (left). The enamel-dentine junction of the tooth shows the mesiodistal convexity (a), the lingual crests and fossae (b) and an enamel fracture on the distal side of the crown (c). Abbreviations: O = occlusal; B = buccal; l = lingual; d = distal; m = mesial. Scale bar = 1 cm.

2. Materials and methods

This item was downloaded from IRIS Università di Bologna (<https://cris.unibo.it/>)

When citing, please refer to the published version.

2.1 Comparative sample

A comparative set of upper deciduous canines including Neanderthals (NEA; $n = 12$) and Upper Paleolithic and Mesolithic *H. sapiens* (UPMHS; $n = 91$; Frayer, 1978; Voisin et al., 2012) was integrated using an unpublished comparative sample (Max Planck Institute collection) gathered for this study—comprising Neanderthal (NEA; $n = 5$), early *Homo sapiens* (EHS; $n = 2$), and Upper Paleolithic *H. sapiens* (UPHS; $n = 2$; see Supplementary Online Material [SOM] Table S1). Moreover, a set of recent *H. sapiens* (RHS; $n = 20$) upper deciduous canines was acquired at the University of Ferrara by means of a μ CT system.

2.2. Microtomographic acquisition and postprocessing

High-resolution μ CT images of the upper deciduous canine RB1 were obtained through a semiengineered rotating gantry μ CT scanner with variable geometry (Xalt; Panetta et al., 2012). The tooth was scanned at 50 peak kilovoltage (kVp), 1 mm Al filtration, with 960 projections over 360° and 0.9 mA·s/projection. The total scan time was 48 min. The tomographic images were reconstructed using a modified Feldkamp algorithm (Feldkamp et al., 1984) with embedded compensation for mechanical misalignments and raw data pre-correction for beam-hardening and ring artifacts reduction. Raw images were reconstructed into a volume dataset of $768 \times 768 \times 1024$ cubic voxels (18.4 μ m size).

A set of recent *H. sapiens* (RHS; $n = 20$) upper deciduous canines was acquired (voxel size of 30 μ m) at the University of Ferrara. The teeth were scanned at 70 kVp, 0.25 mm Al filtration, 360 projections over 360° , 0.5 mA·s/projection for a total scan time of 30 min per sample. Alignment optimization, beam-hardening, and ring artifact corrections were performed by computer program using a modified Feldkamp algorithm (Feldkamp et al., 1984). The μ CT volumes were segmented using Avizo 9.2 software (Thermo Fisher Scientific, Waltham, Massachusetts, US). The 3D models

This item was downloaded from IRIS Università di Bologna (<https://cris.unibo.it/>)

When citing, please refer to the published version.

of the dental tissues (i.e., enamel, dentine and the preserved portion of the pulp chamber) were refined in Geomagic Design X (3D Systems Software, Rock Hill, South Carolina, US) to optimize the triangles and create fully closed surfaces.

2.3. Morphological description

The morphological description of RB1 was performed according to standards outlined by the Arizona State University Dental Anthropology System (ASUDAS; Turner et al., 1991). The wear stage of the occlusal surface was assessed based on Molnar (1971; SOM Table S1). The age of root resorption was estimated combining different observations, such as stages of tooth formation, dental eruption and root resorption using the sequences based on modern human standard provided by Moorrees (1963) and Al Qahtani et al. (2010). In addition, we quantified the degree of morphological expression of three key features observed on the enamel-dentine junction (EDJ) surface, namely the vestibular bulging, the outline asymmetry, and the presence/absence of the mesial crest (SOM Fig. S1). Each non-metric trait was scored according to a discrete scale ranging from 0 (absent) to 3 (marked) with two intermediate stages (1 = slight; 2 = evident), and we assigned the observed degree to each individual in our reference sample (SOM Table S2). Frequencies of each trait in RHS, EHS and NEA subsamples were calculated considering a trait as present if the associated score was greater than or equal to 1. The UPHS sample was excluded because heavily worn.

2.4. Metric comparisons

Each tooth was oriented with the best-fit plane computed at the cervical line (i.e., the cervical plane that best fits a spline curve digitized at the cervical line), parallel to the xy-plane of the Cartesian coordinate system (as described in, e.g., Benazzi et al., 2013; Been et al., 2017; Fiorenza et al., 2018) and rotated along the z-axis to have its lingual aspect parallel to the x-axis (Fig. 3). The size of the

This item was downloaded from IRIS Università di Bologna (<https://cris.unibo.it/>)

When citing, please refer to the published version.

bounding box enclosing the crown and cervical outlines were used to collect mesiodistal (MD) and buccolingual (BL) diameters, following the approach published by Benazzi et al. (2013), Margherita et al. (2016, 2017), and Been et al. (2017).

The bidimensional topographic variation of enamel thicknesses, on both the buccal aspect of RB1 and in the comparative sample, was measured using the free software package MPSAK v.2.9 (Dean and Wood, 2003) on virtual sections along the buccolingual plane and through the longitudinal mid-axis of the teeth (SOM Fig. S2). Enamel thickness was measured between the EDJ and the outer enamel surface, from the neck to the most apical preserved enamel, at 100 μm intervals. To reduce the effect of tooth size, linear enamel thicknesses were standardized with the bicervical diameter measured on the same section of each tooth (Macchiarelli et al., 2007; Le Luyer et al., 2014). The lingual aspect was not taken into consideration because affected by the high morphological variability of the EDJ shape (Fig. 4).

To compare the same sampling points across all individuals, enamel thickness values were also taken at the first, second (median), and third quartile of the distance between the cervical plane and the 100 μm bin closest to the bicervical diameter (Fig. 5). Differences in the distribution of enamel thickness between Neanderthal and RHS was then tested through one-tailed Mann-Whitney tests for each quartile (null hypothesis assumed that Neanderthals had lower values than RHS).

The presence of significant differences in the distribution of both crown and cervical BL and MD diameters among fossil and extant human groups (with the exclusion of RB1) was first assessed through a non-parametric Kruskal-Wallis test, and further investigated through two-tailed pairwise Mann-Whitney tests for independent study design. Observed diameter values were used for individuals who presented with either the left or right upper canine, while for individuals presenting with both antimeres we estimated and used the mean between the left and right tooth. The effects of multiple testing were controlled via a Bonferroni correction. Effect size between RHS and NEA was

This item was downloaded from IRIS Università di Bologna (<https://cris.unibo.it/>)

When citing, please refer to the published version.

calculated for both crown and cervical BL and MD diameters, while effect size between UPMHS and NEA was calculated only for crown diameters. In all cases we used Cohen's *d* for unpaired samples with pooled standard deviation and Hedge's correction for small sample size via the function `cohen.d` of the package `effsize` in R (R Core Team, 2018; Torchiano, 2018). We tested for normality of crown and cervical BL and MD diameters in RHS, UPMHS, and NEA through a Shapiro-Wilk test. Power analysis for an unpaired *t* test with unequal sample sizes between RHS and NEA was also run for all the above-mentioned variables, while the same analysis was run for crown diameters between RHS and NEA as well as between UPMHS and NEA using the function `pwr.t2n.test` of the package `pwr` in R (Champely, 2018). The measure obtained for RB1 crown BL and MD diameters were visually compared against 95% confidence intervals calculated for NEA, UPMHS and RHS, and with individual measures obtained for EHS. Cervical diameters measured on RB1 were compared against individual values plotted for EHS and UPHS specimens. We finally measured the probability that RB1 falls within the range of variability of crown BL diameter, cervical BL diameter, and cervical MD diameter attributed to RHS, and within the range of crown BL estimates for UPMHS, through a one-tailed *t*-test for comparison of a single observation with the mean of a sample (following Sokal and Rohlf, 1995 and Madrigal, 2012). The alternative hypothesis was that each individual diameter measured for RB1 could be significantly higher than the mean respective value calculated for recent and fossil modern humans.

Morphological variability was further explored by computing the relative frequency of each morphological trait (vestibular bulging, outline asymmetry and mesial crest) in RHS, EHS and NEA, and calculating a pairwise Morisita-Horn index of overlap (via the function `sim.table` in the package `vegetarian` in R; Charney and Record, 2012; Jost, 2007). The inverse of such index was used in a hierarchical cluster analysis performed using Ward's method to visually inspect proximity between groups.

This item was downloaded from IRIS Università di Bologna (<https://cris.unibo.it/>)

When citing, please refer to the published version.

A new index (hereafter called coronal pulp index) was computed in order to overcome limitations and alterations produced by dental wear on the incisal surface. In detail, the crown dentine was isolated from the root by using the spline curve digitized at the cervical line, which was then closed by interpolating the curve with a smooth surface (Benazzi et al., 2014a). A plane (offset plane) was drawn parallel to the cervical plane, passing through the highest point of the crown pulp chamber—differently to what proposed by Benazzi et al. (2011b) for molars, where the plane was set at the lowest point of the EDJ in the mid-occlusal basin. The region of the crown between the two planes (i.e., cervical and offset plane) was used to measure the lateral enamel volume, lateral dentine volume, and coronal pulp volume (Fig. 3). The latter two tissues were used to calculate the coronal pulp index as follows: $\text{coronal pulp volume} / \text{lateral dentine volume without pulp} * 100$. Differences in coronal pulp index values between NEA and RHS were also ascertained through two-tailed Mann Whitney tests.

Even though RB1 did not provide reliable information for the computation of 2D and 3D average and relative enamel thickness (AET and RET, respectively) due to its heavily worn condition and a crown fracture, 3D AET/RET (Benazzi et al., 2014a) and 3D lateral AET/RET (Benazzi et al., 2011b)—suitably modified considering the highest point of the crown pulp chamber rather than the lowest point of the EDJ in the mid-occlusal basin) were calculated on the comparative sample to provide a comprehensive database for deciduous upper canines. The 3D AET index (in mm) is the enamel volume divided by the underlying EDJ surface, while the 3D RET index (scale-free) is the 3D AET divided by the cube root of the crown dentine and pulp volumes. As far as the lateral enamel thickness is concerned, we considered the region of the crown between the two planes mentioned above (i.e., cervical and offset planes). The 3D lateral AET index (in mm) is the lateral enamel volume divided by the underlying EDJ surface, while the 3D lateral RET index (scale-free) is the 3D lateral AET divided by the cube root of the lateral crown dentine and pulp volumes.

This item was downloaded from IRIS Università di Bologna (<https://cris.unibo.it/>)

When citing, please refer to the published version.

Differences in the distribution of 3D lateral RET values between NEA and RHS were ascertained through two-tailed Mann Whitney tests. As far as the 3D RET is concerned, the small sample size discouraged any statistical analysis.

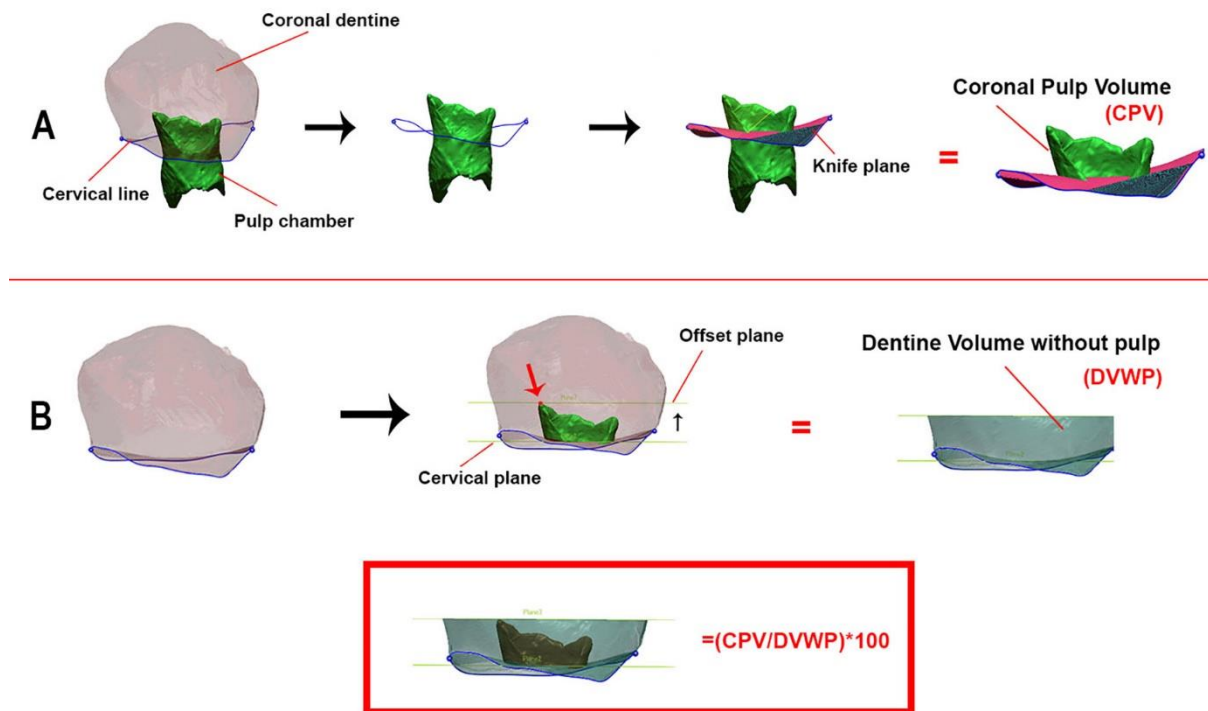


Figure 3. Pulp chamber volume. A) A spline curve was digitized at the cervical line to isolate the crown dentine, which was then closed by interpolating the curve with a smooth surface (knife plane). This surface was used to trim the upper area of the pulp chamber (coronal pulp chamber). B) A plane (offset) was drawn parallel to the cervical plane, passing through the highest point of the crown pulp chamber. Dentine volume without pulp was the region used to measure the coronal pulp index, i.e., the coronal pulp volume divided by the lateral dentine volume.

This item was downloaded from IRIS Università di Bologna (<https://cris.unibo.it/>)

When citing, please refer to the published version.

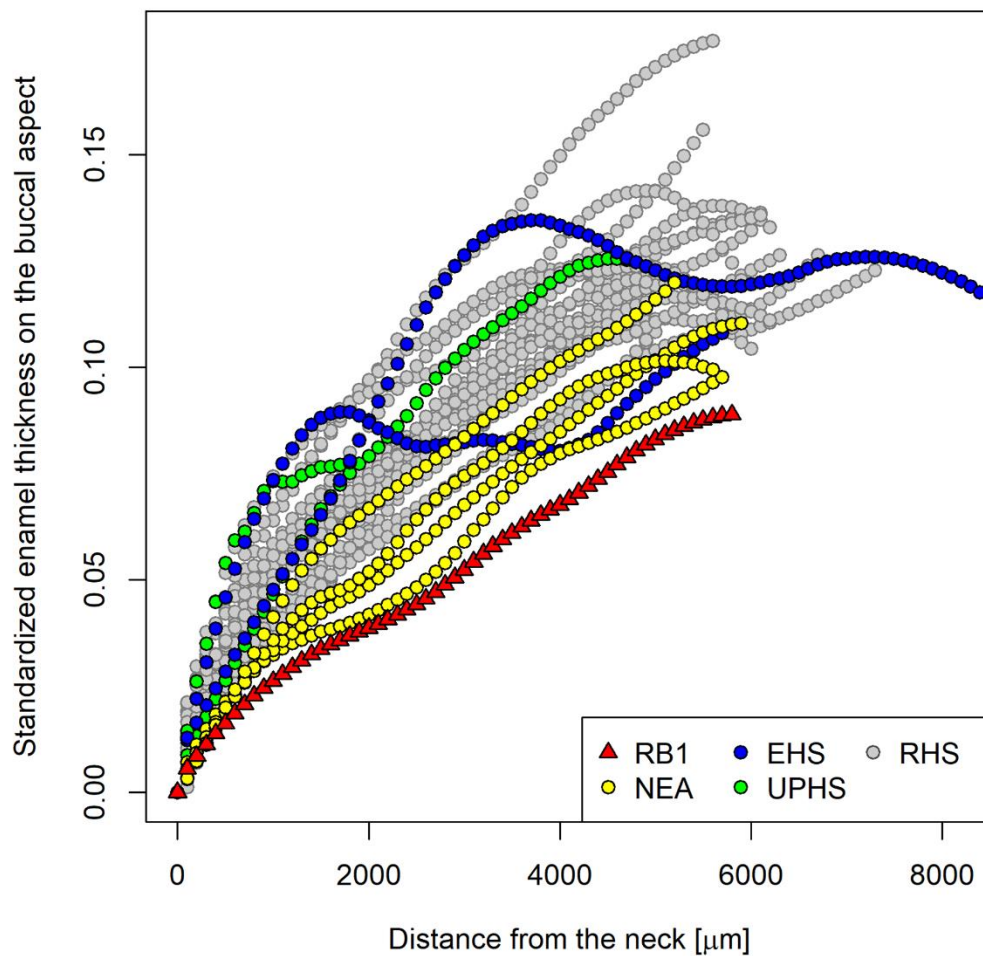


Figure 4. Patterns of standardized enamel thickness variation in the buccal aspect of Riparo Broion 1 (RB1) and of the deciduous canine comparative set. Abbreviations: NEA = Neanderthals; EHS = early *Homo sapiens*; UPHS = Upper Paleolithic *H. sapiens*; RHS = recent *H. sapiens*. See text for details on measurements and standardization.

This item was downloaded from IRIS Università di Bologna (<https://cris.unibo.it/>)

When citing, please refer to the published version.

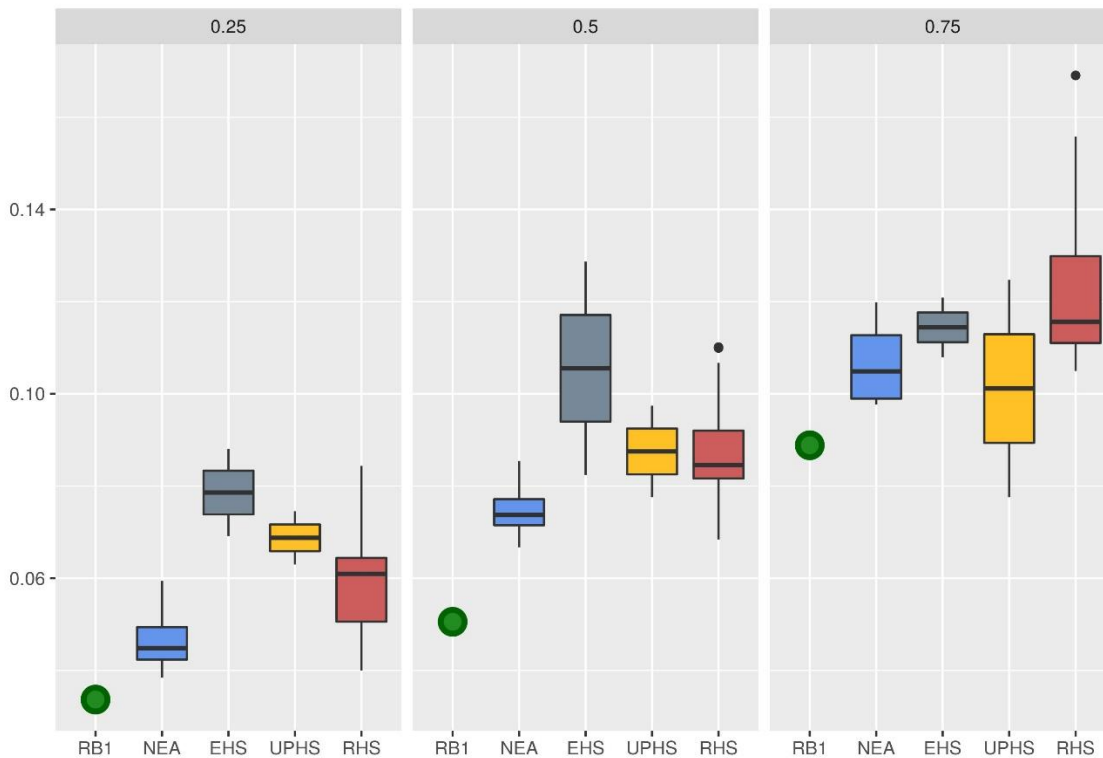


Figure 5. Box plots comparing the distribution of enamel thickness measured at 25%, 50%, and 75% of the distance between the cervical plane and the 100 μm bin closest to the bicervical diameter in Riparo Broion 1 (RB1), Early Homo sapiens (EHS), Neanderthals (NEA), recent *H. sapiens* (RHS), and Upper Paleolithic *H. sapiens* (UPHS) in the present sample. The value corresponding to RB1 (single observation) is indicated by a green dot, while the distribution of values measured in other groups are depicted as boxes representing 50% of all observations, i.e. those with values comprised between the first (lower limit) and third (upper limit) quartile, and whiskers which extend to values located in the lowermost and uppermost quarters of the distribution up to values as high as 1.5 times the interquartile range. Outlier points represent maximum values located beyond this threshold. Solid black lines in each box indicate median values.

2.5. DNA analysis

After removing a thin layer (~ 1 mm) from a small area of the root surface and obtaining a sample of dentine, 500 μl of lysis buffer were added to 5 mg of material. Three DNA extracts were prepared from 150 μl -aliquots of the lysate on a Bravo NGS workstation (Agilent Technologies) using silica-coated magnetic beads and binding buffer ‘D’ as described elsewhere (Rohland et al., 2018). Extracts were converted into single-stranded libraries with an automated version of a protocol using T4 DNA

This item was downloaded from IRIS Università di Bologna (<https://cris.unibo.it/>)

When citing, please refer to the published version.

ligase for the ligation of both adapters (Gansauge et al., 2017). Quantitative PCR (qPCR) assays were carried out to quantify the number of molecules in the libraries (Gansauge and Meyer, 2013) and to evaluate the efficiency of the library preparation procedure (Glocke and Meyer, 2017). More details can be found in SOM S1.

We used a hybridization capture method to enrich human mitochondrial DNA fragments from an aliquot of each indexed DNA library (Maricic et al., 2010). The enriched libraries were then sequenced on an Illumina MiSeq platform in 76-cycle paired-end runs (Kircher et al., 2012). For a detailed description of the read processing, see SOM S1–S3. We aligned sequences to the revised Cambridge reference sequence (rCRS; Andrews et al., 1999) or the mitochondrial sequence of Spy 94a (Hajdinjak et al., 2018) using parameters adjusted for ancient DNA (Meyer et al., 2012). To estimate present-day human DNA contamination, we identified 48 positions where the mitochondrial genomes of 312 present-day humans (Green et al., 2008; including rCRS) and 23 Neanderthals (Green et al., 2008; Briggs et al., 2009; Gansauge and Meyer, 2014; Prüfer et al., 2014; Skoglund et al., 2014; Brown et al., 2016; Rougier et al., 2016; Hajdinjak et al., 2018; Peyrégne et al., 2019) differ, and computed for each library the proportion of sequences that carry the present-day human allele at these positions. The partial mitochondrial genome sequence of RB1 was reconstructed from a consensus call at positions covered by at least five sequences and where at least 80% of the sequences carry the same allele. Some positions with a consensus support lower than 80% could be resolved by calling a consensus base solely from sequences that exhibit cytosine to thymine (C-to-T) substitutions within the last three positions of either end.

We used BEAST2 (Bayesian Evolutionary Analysis Sampling Trees v. 2.6.1; Bouckaert et al., 2014) to build a phylogenetic tree relating the mtDNA of RB1 to 54 present-day (Ingman et al., 2000) and 38 ancient humans including 23 Neanderthals (Green et al., 2008; Briggs et al., 2009; Gansauge and Meyer, 2014; Prüfer et al., 2014; Skoglund et al., 2014; Brown et al., 2016; Rougier et al., 2016;

This item was downloaded from IRIS Università di Bologna (<https://cris.unibo.it/>)

When citing, please refer to the published version.

Hajdinjak et al., 2018; Peyrégne et al., 2019), 4 Denisovans (Krause et al., 2010a; Reich et al., 2010; Sawyer et al., 2015; Slon et al., 2017), one hominin from Sima de los Huesos (Meyer et al., 2014) and 10 early modern humans (Ermini et al., 2008; Gilbert et al., 2008; Krause et al., 2010b; Fu et al., 2013a, 2013b, 2014). We identified the best fitting substitution model using jModelTest 2.1.10 and the best fitting clock and tree models using the MODEL_SELECTION package of BEAST2 (Bouckaert et al., 2014). We used three Markov Chain Monte Carlo runs of 75,000,000 iterations, sampling parameter values and trees every 5,000 iterations. A detailed description of this analysis can be found in the SOM S4. The sequencing data generated for this project was deposited in the European Nucleotide Archive (<https://www.ebi.ac.uk/ena>, accession number PRJEB35184).

2.6. Radiocarbon dating

All bones selected for dating were anthropically marked (Table 1). They were dated at the Oxford Radiocarbon Accelerator Unit (ORAU), University of Oxford, using established protocols (Higham et al., 2006; Brock et al., 2010) based on the ultrafiltration of gelatinized bone collagen (Brown et al., 1988) to remove low molecular weight contaminants (Brock et al., 2010). Radiocarbon ages are provided as conventional ages BP after Stuiver and Polach (1977) in Table 1 with BP representing radiocarbon years before present (1950 AD). We also provide our results in fM (fraction modern) notation and use this for the purpose of calibration (Reimer et al., 2013). We subtracted a bone-specific background after Wood et al. (2010) for all samples down to ~5 mg of collagen. We measured C:N atomic ratios, % weight collagen, %C on combustion, %N and stable isotopic values (Table 1). Two samples yielded sufficiently well-preserved collagen (both with OxA- numbers). Two others showed very poor yields (i.e., less than the ideal minimum of 5 mg of collagen). These were given OxA-X- numbers. The %carbon values are also very low compared with the average expected values (~42–45%) and for this reason these two samples were pretreated using the AG (gelatinization)

This item was downloaded from IRIS Università di Bologna (<https://cris.unibo.it/>)

When citing, please refer to the published version.

method instead of ultrafiltration. We therefore consider the resulting dates as most likely minimum ages. Despite the few results at hand, we incorporated the chronometric results into a basic Bayesian phase model to consider the results with respect to stratigraphic phasing (see Higham et al., 2014 for details). We used OxCal (Bronk Ramsey, 2009) and the IntCal13 dataset (Reimer et al., 2013).

Table 1

Radiocarbon determinations obtained from Riparo Broion and associated analytical data.

OxA ^a	PCode ^b	Used (mg) ^c	Yield (mg) ^c	%Yld ^c	%C ^d	$\delta^{13}\text{C}$ (‰) ^e	$\delta^{15}\text{N}$ (‰) ^e	CN ^f	CRA	±	F14C	±
OxA-X-2792-24	AG	721	3.61	0.5	35.1	-20.8	5.4	3.2	37800	1200	0.00899	0.00133
OxA-X-2792-25	AG	746	2.17	0.3	23	-20.0	5.7	3.3	37000	1900	0.00995	0.00231
OxA-35527	AF	780	10.3	1.3	43.1	-19.8	9.0	3.2	38900	1000	0.00793	0.00101
OxA-37959	AF	763	22.04	2.9	44.8	-21.4	2.8	3.2	48100	3100	0.00249	0.00098

Abbreviations: PCode = pretreatment code; %Yld = percent yield; CRA = conventional radiocarbon age (BP); F14C = fraction modern ¹⁴C.

^a OxA-X- prefixes denote either an unusual experimental pretreatment chemistry or caution recommended to the measurement. In this case it is the latter due to low collagen yields and %C on combustion. The bones were all humanly modified: OxA-X-2792-24 (US 9) was a bone flake derived from impact; OxA-X-2792-25 (US 9) and OxA-37959 (US 11 lower) were small bones with percussion evidence; OxA-35527 (level 1g) was the diaphysis fragment of a herbivore with a percussion cone.

^b AG = unfiltered and gelatinized collagen extracted from the bones after Brock et al. (2010); AF = ultrafiltration protocol applied in Oxford.

^c Yield represents the weight of ultrafiltered collagen in milligrams. %Yld is the percent yield of extracted collagen as a function of the starting weight of the bone analyzed ('used' also in mg).

^d %C is the carbon present in the combusted gelatin.

^e Stable isotope ratios are presented in ‰ relative to VPDB and AIR with a mass spectrometric precision of $\pm 0.2\text{‰}$ for C and $\pm 0.3\text{‰}$ for N.

^f CN is the atomic ratio of carbon to nitrogen. It is acceptable if it ranges between 2.9–3.5 (Brock et al., 2010).

This item was downloaded from IRIS Università di Bologna (<https://cris.unibo.it/>)

When citing, please refer to the published version.

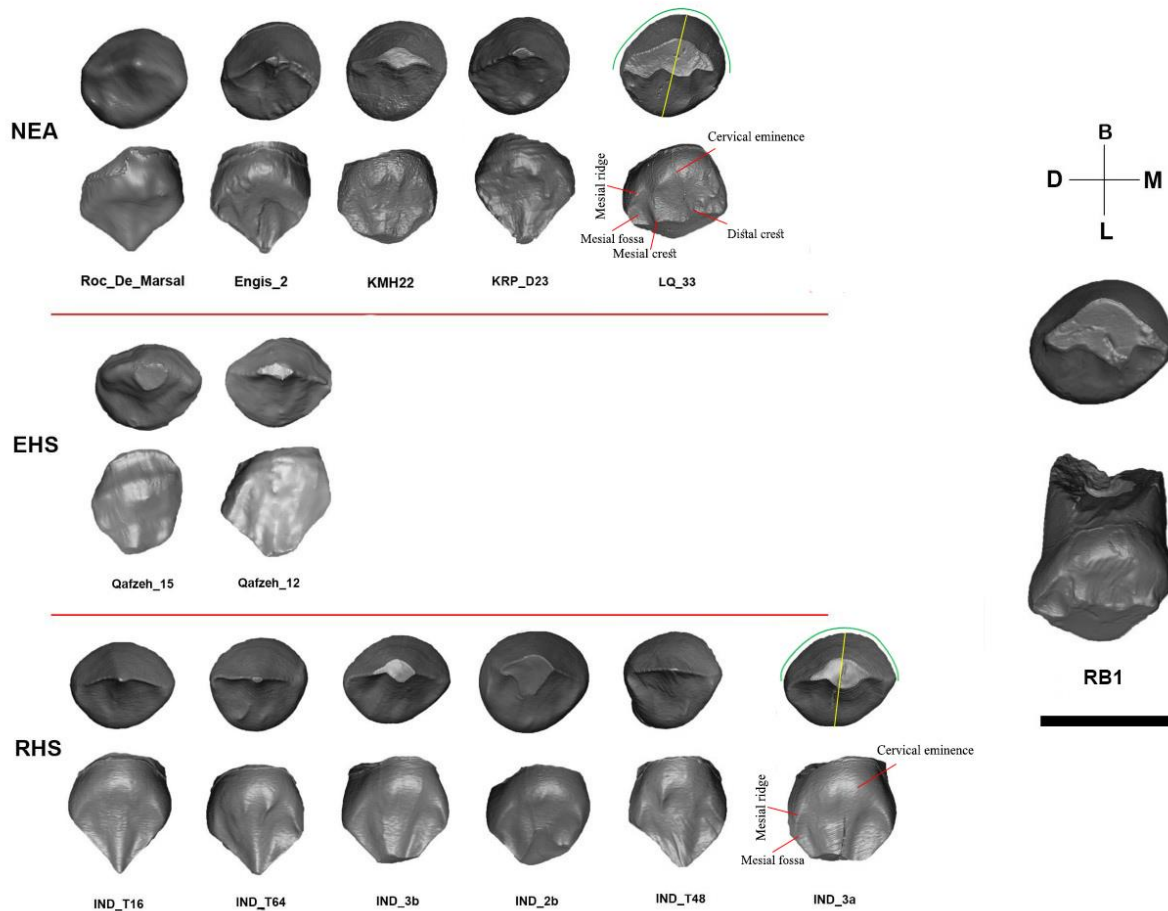


Figure 6. Enamel-dentine junction of individuals belonging to the comparative sample composed by Neanderthals (NEA), early *H. sapiens* (EHS) and recent *Homo sapiens* (RHS). On the right side, the EDJ of Riparo Broion 1. Some teeth have been flipped in order to facilitate morphological comparison among species and Riparo Broion 1: Roc de Marsal (NEA), Engis2 (NEA), T16 (RHS), T48 (RHS), 3a (RHS), T64 (RHS), KMH22 (Kebara, NEA), KRP_D23 (Krapina, NEA). Scale bar = 1 cm

This item was downloaded from IRIS Università di Bologna (<https://cris.unibo.it/>)

When citing, please refer to the published version.

3. Results

3.1. Morphological description

RB1 is an exfoliated right upper deciduous canine (dC¹), with a fractured crown and about one-fourth of the root preserved (Fig. 2). As far as pathological conditions are concerned, neither caries nor enamel hypoplasia are visible. The enamel shows some fractures from the cervix to the incisal margin. Dentine tissue is visible on the distal side of the crown due to a large fracture of the enamel (length = 3.20 mm; breadth = 3.35 mm). The fractures, however, do not affect the underlying dentine which was used to obtain cervical MD diameters. The incisal edge is worn obliquely, from mesiobuccal to distolingual, exposing a large area of dentine (wear stage 4 according to Molnar, 1971). The tooth crown has a BL diameter of 6.84 mm (SOM Table S3), whereas BL and MD cervical diameters are 6.22 mm and 6.23 mm, respectively (SOM Table S4). The preserved root, slightly more elongated buccally (mid-buccal height = 3.71 mm) than lingually (mid-lingual height = 1.29 mm), is resorbed (stage Res3/4 of Moorrees, 1963), suggesting an age at exfoliation of approximately 11–12 years on the basis of recent human standards (Al Qahtani et al., 2010).

Overall, the crown is bulging on the buccal side (vestibular convexity equal to ASUDAS grade 4). Observing from the incisal view, the crown appears asymmetrical due to a distolingual projection of a lingual cervical eminence. From the cervix, the crown flares mesially, while it raises almost vertically on the distal side, possibly accentuated by the lack of enamel on this side of the crown. While on the external surface most of the dental traits were removed by tooth wear, remnants of lingual crests are still visible at the EDJ (SOM Fig. S1). More specifically, two moderately expressed mesial and distal crests delimit a shallow central fossa, while the mesial crest and the mesial marginal ridge delimit a mesial fossa (Fig. 4, right panel).

As shown in Figure 6, Neanderthals and *H. sapiens* show different features at the EDJ. From the incisal view, Neanderthals are characterized by a strong buccal bulging of the crown and a concave

This item was downloaded from IRIS Università di Bologna (<https://cris.unibo.it/>)

When citing, please refer to the published version.

lingual side with a cervical, distolingually-directed eminence or tubercle, which contribute to produce an asymmetrical outline. Based on our comparative sample, the lingual wall often shows crests and a mesial fossa distally limited by a mesial crest, which are less frequently observed in our *H. sapiens* sample. Indeed, in EHS and RHS (Fig. 6; SOM S5), the crown is less rounded, more flattened buccolingually due to the reduced expression of the lingual eminence or tubercle, and has a more symmetric outline (from the incisal view) than in Neanderthals. Therefore, the combined presence of these features (vestibular bulging, asymmetric outline, mesial crest) aligns RB1 with Neanderthals. This conclusion is supported by measures of overlap between groups and based on the frequency of the observed morphological traits, which show that RB1 is morphologically closer to NEA and that both groups are more similar to RHS than to EHS (SOM S5 and S6).

3.2. Morphometric comparison

BL crown diameter of RB1 (6.84 mm) is notably greater than those measured for RHS (BL: mean = 6.10, SD = 0.40) and UPMHS (mean = 6.23, SD = 0.47), smaller than the diameters measured for EHS (BL: mean = 7.17., SD = 0.43), and falls within the Neanderthal range of variation (BL: mean = 6.86, SD = 0.54), close to Roc de Marsal and La Quina (LQ33; Table 2; SOM Table S3; SOM S7). We found significant differences between RHS and NEA for all the examined diameters (i.e., crown BL diameter, cervical BL diameter, crown MD diameter, and cervical MD diameter; SOM S8). Both crown diameters were also found to be significantly different between NEA and UPMHS (SOM S8).

Effect size and statistical power for the difference between NEA and RHS, as well as between NEA and UPMHS are large for all the considered measures (SOM S9–S11). Crown BL diameter, cervical BL diameter, and cervical MD diameter of RB1 (Table 2) are significantly higher than the upper limit of the present RHS group range (SOM S12; SOM Tables S3 and S4), while the crown BL diameter of RB1 is not significantly higher than the range recorded for UPMHS (SOM S12). Values

This item was downloaded from IRIS Università di Bologna (<https://cris.unibo.it/>)

When citing, please refer to the published version.

recorded for RB1 consistently fall within the 95% confidence intervals calculated for the same measures in NEA and are always close to values attributed to EHS specimens (SOM Figs. S3 and S4).

Table 2

Crown and cervical measurement of Riparo Broion 1 tooth (RB1) and individuals belonging to the comparative sample. Each row reports group mean and SD (in parentheses).

	MDCrown	BLCrown	MDCervical	BLCervical
RB1	NA	6.84	6.23	6.22
NEA	7.59 (0.62)	6.86 (0.54)	6.04 (0.34)	6.27 (0.32)
EHS	8.28 (0.50)	7.17 (0.43)	6.1 (0.42)	5.89 (0.23)
UP(M)HS	6.95 (0.48)	6.23 (0.47)	5.38 (0.11)	5.25 (0.28)
RHS	6.94 (0.47)	6.10 (0.40)	5.27 (0.42)	5.39 (0.34)

Abbreviations: NEA = Neanderthals; EHS = early *Homo sapiens*; UP(M)HS = Upper Paleolithic (and Mesolithic only for crown diameters) *H. sapiens*; RHS = recent *H. sapiens*; MDCrown = mesiodistal crown length; BLCrown = buccolingual crown width; MDCervical = mesiodistal cervical length; BLCervical = buccolingual cervical width.

Figure 4 depicts the patterns of standardized 2D enamel thicknesses variation (buccal aspect) in RB1 and the comparative set. Engis 2 was excluded from the analysis due to the absence of enamel in the cervical third of the buccal aspect.

The Neanderthal group shows the lowest standardized enamel thicknesses compared to *H. sapiens*, both fossil and extant. However, the Neanderthal Krapina D23 (KRP_D23) falls inside the RHS range of variation. The UPHS individuals fit inside the upper levels of the RHS range. The EHS individuals (Qafzeh 12 and 15) exhibit the thickest enamel. Shapes of EHS profiles are different compared to the shapes of the other groups, showing a relative expansion in the middle and cervical third of the crown. RB1 shows the lowest standardized enamel thickness profile in the whole comparative fossil and

This item was downloaded from IRIS Università di Bologna (<https://cris.unibo.it/>)

When citing, please refer to the published version.

extant *Homo* dataset. Significant differences in the distribution of enamel thickness emerged between NEA and RHS at 25%, 50%, and 75% of the distance between the cervical plane and the 100 µm bin closest to the bicervical diameter (Fig. 5; SOM Table S5). RB1 is close to Neanderthals at 25% and 50%, while it overlaps with UPHS values at 75% (Fig. 5).

As far as coronal pulp index is concerned (SOM Table S4), it shows no significant differences ($W = 34$, $p = 0.3$; SOM S13) between NEA (mean = 8.92, SD = 5.39) and RHS (mean = 12.11, SD = 4.87). However, even though Neanderthal mean values show an overlap with RHS values, it is clear that the coronal pulp index of the former group tends to be smaller than the one measured for RHS. In light of this consideration, RB1 (coronal pulp index = 4) might be considered out of the RHS range and comparatively closer to Neanderthals.

3D lateral RET index did not provide any significant result between the NEA and RHS (LatRET: $W = 25$, $p = 0.0969$; SOM S14; SOM Table S6). As far as 3D RET is concerned, increasing of wear pattern on the occlusal surface seems to produce a reduction of 3D RET for each human group (SOM Table S6). Moreover, even though it was not possible to perform statistical analysis, differences can be appreciated in 3D RET values between NEA and RHS where Neanderthals show lower mean values (for each wear stage) than RHS.

3.3. DNA analysis

Following the preparation of DNA libraries (SOM Table S7) from the specimen and their enrichment for hominin mitochondrial DNA fragments, we obtained 54,540 unique sequences that align to the human mitochondrial reference genome (~154 fold average coverage), including 20,747 sequences that exhibit signs of ancient DNA damage (Briggs et al., 2007) within the first or last three positions (~57 fold average coverage; SOM Tables S8 and S9). Using diagnostic positions that differ between the mitochondrial genomes of present-day humans and Neanderthals (Green et al., 2008),

This item was downloaded from IRIS Università di Bologna (<https://cris.unibo.it/>)

When citing, please refer to the published version.

we found that 83.9% of the retrieved sequences overlapping such positions exhibit the Neanderthal state (SOM Table S10). This suggests that the mitochondrial genome of this individual falls into the Neanderthal mitochondrial variation and that 16.1% of the sequences represent present-day human DNA contamination (95% binomial confidence interval = 14.6–17.8%). Because contaminant sequences represent a minority of the retrieved sequences, we were able to assemble a partial mitochondrial genome from the ancient individual (44 unresolved positions; see Materials and methods and SOM S3).

We then applied a Bayesian method for phylogenetic tree inference (Bouckaert et al., 2014) to assess how this mitochondrial genome relates to other Neanderthal mitochondrial sequences (SOM Tables S11 and S12). We found that it is most closely related to the published sequences from the Spy and Goyet Neanderthals from Belgium who lived between 38 and 43 ka cal BP (Rougier et al., 2016; Hajdinjak et al., 2018; Fig. 7). The number of mutations they share allowed us to date their last common mitochondrial ancestor to 47 ka (95% highest posterior density interval [HPDI] = 43–51 ka). Finally, by comparing the branch lengths of RB1 and other Neanderthals in the tree, we estimated the age of RB1 to be close to 39 ka (95% HPDI = 30–46 ka).

3.4. Radiocarbon dating

The radiocarbon dating results (Fig. 8) are consistent and there are no outliers of significance. The posterior probability distribution assigned by the Bayesian age model to the lower portion of unit 11 ranges from 50,000 to 45,700 cal BP (95% CI).

4. Discussion and conclusions

RB1 is a right dC¹ with an incomplete crown and bulged buccal wall, an asymmetric outline due to a distolingually-directed lingual eminence (from the incisal view), and a complex morphology in

This item was downloaded from IRIS Università di Bologna (<https://cris.unibo.it/>)

When citing, please refer to the published version.

the lingual aspect of the EDJ (crests and fossae). As pointed out above (see also Fig. 5), these features are typically observed in Neanderthals and allow RB1 to be assigned to this human group. Moreover, the standardized enamel thickness of RB1 falls within the Neanderthal range of variability, which is significantly lower than the range observed for RHS.

Because of the advanced wear stage of RB1, we made use of a digital comparative sample to attempt a taxonomic discrimination based on the coronal pulp index, a new index computed by dividing the pulp crown volume by the crown dentine volume. Unfortunately, this index did not allow to discriminate between Neanderthal and modern human upper deciduous canines. Nonetheless, the index we provide can be used in future studies concerning the same or different tooth classes and offer additional means for taxonomic discrimination between groups.

Despite being unhelpful for the taxonomical assessment of RB1, this study offers the first available morphometric reference sample for the distribution of enamel thickness in upper deciduous canines of both modern humans and Neanderthals. Owing to the general worn condition of the dental hominin fossil record, besides computing the 3D AET/RET indices from the complete crown, we decided to quantify the 3D lateral AET/RET indices, taking advantage of the two planes opportunely created to identify the crown pulp volume. Unfortunately, at least based on our sample, the 3D lateral RET index does not seem to be useful to discern this tooth position (dC^1) between Neanderthals and modern humans. Conversely, despite the small sample size, the 3D RET computed from the entire crown seems promising for taxonomical discrimination between the two human groups, at least for moderately worn upper deciduous canines. However, additional work is needed to fully explore the discriminant power of enamel thickness in deciduous canines.

Considering the high discriminant power observed for crown and cervical diameters, morphometric comparisons exclude the attribution of RB1 to a modern human, while general morphology confidently indicate that RB1 belonged to a Neanderthal individual who lived between

This item was downloaded from IRIS Università di Bologna (<https://cris.unibo.it/>)

When citing, please refer to the published version.

48 (Layer 11 lower) and 45 (transition Layer 11 top/9) ka cal BP (Fig. 8; Table 1). Moreover, the reconstructed mtDNA from RB1 also places this individual inside the known Neanderthal mitochondrial diversity.

It is interesting to note that this mitochondrial sequence is remarkably similar to some of the latest Neanderthal individuals uncovered in northern Europe (dated to ca. 43–38 ka, from Spy and Goyet Caves, Belgium; SOM S4; SOM Table S13), with a most recent mitochondrial common ancestor at 47 ka (95% HPDI: 51–43 ka). However future analysis of nuclear DNA is required to determine RB1's relationship with these and other Neanderthals.

Although the presence of modern humans in eastern Europe between ~50–46 ka cal BP has now been confirmed (Richter et al., 2009; Fewlass et al., 2020; Hublin et al., 2020), the vast majority of human remains found in southwestern and Mediterranean Europe in this temporal interval, including RB1 (e.g., La Ferrassie, Le Moustier, and Portel-Ouestin, France; El Salt, El Sidrón, Zafarraya and Sima de las Palomas, Spain; Devil's Tower, Gibraltar; and potentially Lakonis, Greece; Fumane, Italy; and Vindija, Croatia), keep confirming that these regions were, during this time period, still mainly populated by Neanderthals (Wolpoff et al., 1981; Tillier, 1982; Gargett, 1989; Zollikofer et al., 2002; Harvati et al., 2003; Walker et al., 2008; Benazzi et al., 2014b; 2015; Barroso Ruiz et al., 2014; Garralda et al., 2014; Rosas et al., 2017; Gómez-Olivencia et al., 2018; Becam and Chevalier, 2019). While in the rest of Europe (Spy and Goyet in Belgium and Kulna 1 in Czech Republic; Jelinek, 1980; Rougier et al., 2006; Semal et al., 2009) the human remains uncovered in contexts dated between 50–46 ka cal BP are ascribed to individuals of all ages (Becam and Chevalier, 2019), all coeval human fossils uncovered in Italy (with the exception of Fumane 6; Benazzi et al., 2014b) consist of deciduous teeth (Benazzi, 2018).

This item was downloaded from IRIS Università di Bologna (<https://cris.unibo.it/>)

When citing, please refer to the published version.

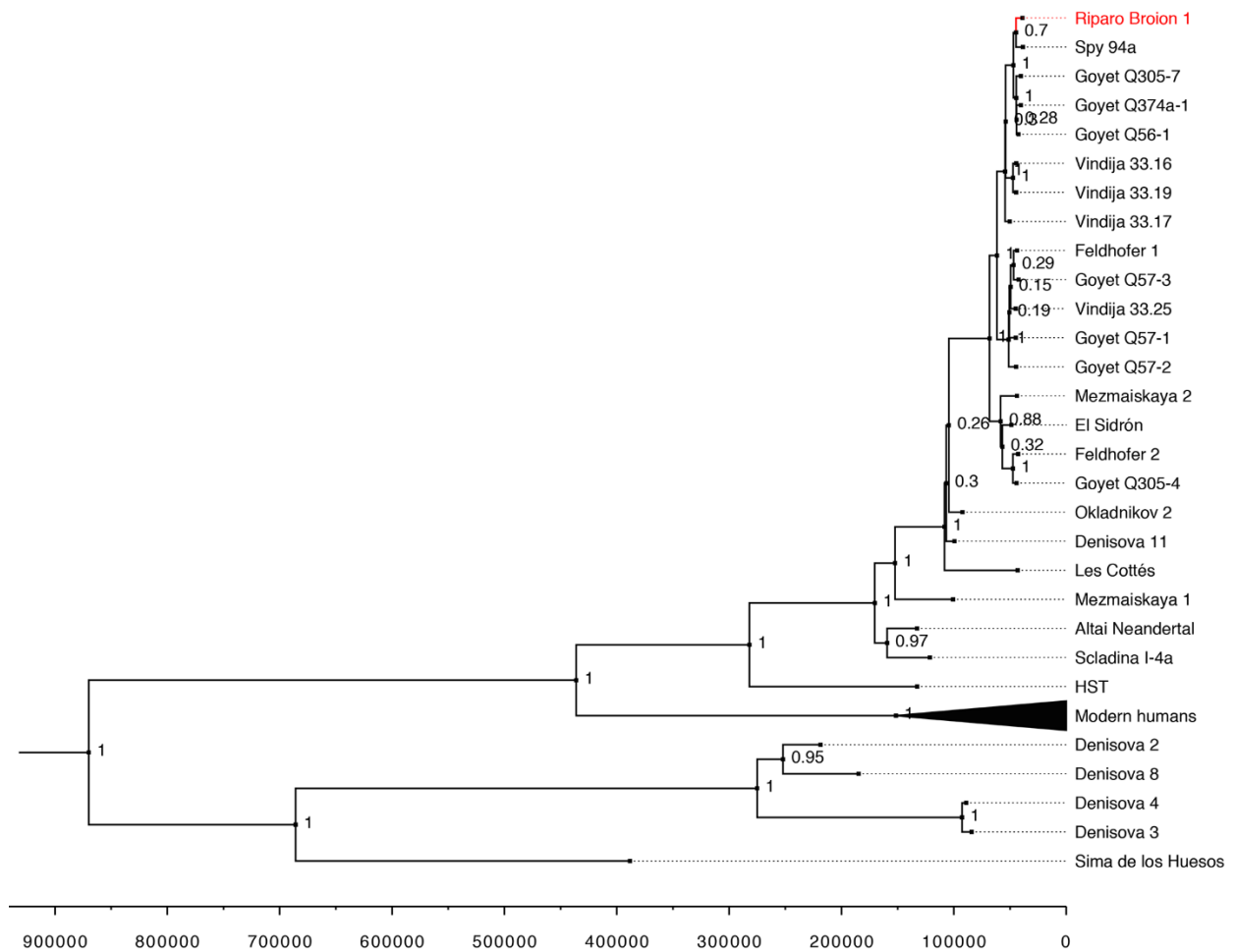


Figure 7. Phylogenetic relationship between the Riparo Broion 1 mitochondrial sequence and currently available archaic and modern human mitochondrial genomes. The tree was reconstructed using BEAST 2. The branch representing the mtDNA of Riparo Broion 1 is in red. The branch representing the mtDNA of a chimpanzee used to root the tree is not shown and the branches corresponding to the modern human mtDNAs were collapsed. The x-axis represents time in years and the numbers at the nodes correspond to posterior probabilities of the depicted branching orders. Abbreviations: HST = Hohlenstein-Stadel Neandertal; El Sidrón = El Sidrón 1253; Les Cottés = Les Cottés Z4-1514; Altai Neandertal = Denisova 5.

This item was downloaded from IRIS Università di Bologna (<https://cris.unibo.it/>)

When citing, please refer to the published version.

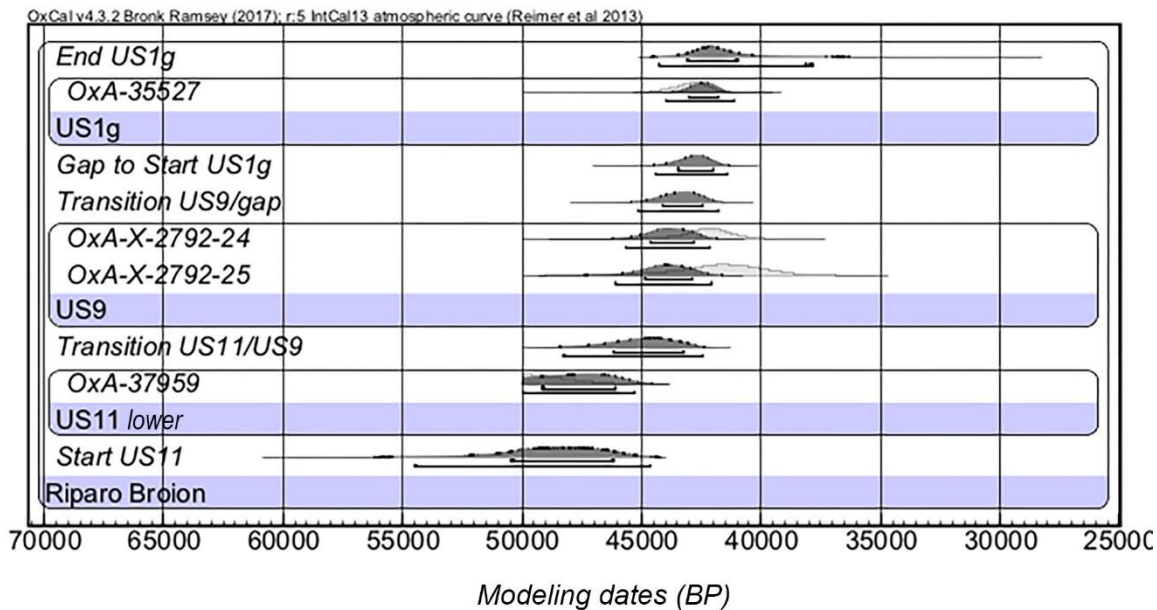


Figure 8. Bayesian age model for Riparo Broion 1. The lighter shaded distributions represent the individual radiocarbon likelihoods. The darker outlines represent the posterior probability distributions, which are the results of the Bayesian modeling.

This pattern is particularly remarkable in the sheltered sites of the Berici Hills and Lessini Mountains. In this region, the high density of faunal bones modified by humans, stone tools, combusted remains, and fire-places points to an intensive (although seasonal) use of caves by human groups, which were likely composed by individuals of all ages (Peretto et al., 2004; Peresani et al., 2011; Romandini et al., 2014, 2019). The preliminary material analysis of Layer 11 at Riparo Broion, together with zooarchaeological (Romandini et al., 2019) and paleoecological information at a regional scale (Badino et al., 2019), yielded evidence of a wide range of Neanderthal activities. For example, cave deposits document an intensive use of fire in a context of environmental conditions ranging from open to dense cool mixed forests, transitional and discontinuous Alpine grasslands, pioneer vegetation on carbonate rocks, surrounded by humid-marshy environments, low energy water courses, wet meadows or shallow lakes.

This item was downloaded from IRIS Università di Bologna (<https://cris.unibo.it/>)

When citing, please refer to the published version.

Outside Italy, in the same interval, the majority of Neanderthal anthropological findings is linked either to inner caves (depth >15m), to possible evidence of cannibalism, or to cave mouths/shelters where archaeologists found plausible or confirmed evidence of deliberate burial (SOM Table S14). For the considered time frame, all evidence collected in Italy to date cannot be linked with certainty to funerary practices, suggesting that diagenesis and taphonomy might also be relevant due to different geomorphological settings of the finding sites (SOM Table S14).

Morphological information, morphometric analysis and ancient DNA analysis show that the Riparo Broion 1 tooth belongs to a Neanderthal child, ultimately adding important to our knowledge of the occupation of northeastern Italy, in a period close to the arrival of modern humans in southern Europe.

Conflict of interest

The authors have no competing interests to declare.

Acknowledgements

Research at Riparo Broion is coordinated by the University of Bologna (M.R.) and the University of Ferrara (M.P.) with the support of the Italian Ministry of Culture, Veneto Archaeological Superintendency SAPAB, the Municipality of Longare, Leakey Foundation (Spring 2015 Grant), and Istituto Italiano di Preistoria e Protostoria. We are grateful to Professor David W. Frayer and the Superintendency of Cremona, Lodi and Mantova (necropolis of Valdaro) for contributing to the reference collection used in this work. This study and related field activities carried out between 2017–2019 received funding from the European Research Council (ERC) under the European Union's Horizon 2020 research and innovation programme (grant agreement No 724046 – SUCCESS, <http://www.erc-success.eu>); the radiocarbon dating was supported by the ERC grant agreement No 324139, PalaeoChron. We thank Elena Essel, Sarah Nagel, Birgit Nickel, Julia Richter,

This item was downloaded from IRIS Università di Bologna (<https://cris.unibo.it/>)

When citing, please refer to the published version.

Barbara Schellbach and Antje Weihmann for help in the lab and Louisa Jauregui for proofreading. We thank the Max Planck Society and the European Research Council (grant agreement number 694707 to Svante Pääbo) for financial support.

References

- Allen, J.R.M., Brandt, U., Brauer, A., Hubberten, H.-W., Huntley B., Keller, J., Kraml, M., Mackensen, A., Mingram, J., Negendank, J.F.W., Nowaczyk, N.R., Oberhänsli, H., Watts, W.A., Wulf, S., Zolitschka, B., 1999. Rapid environmental changes in southern Europe during the last glacial period. *Nature* 400, 740-743.
- Al Qahtani, S.J., Hector, M.P., Liversidge, H.M., 2010. Brief Communication: The London atlas of human tooth development and eruption. *American Journal of Physical Anthropology* 142, 481-490.
- Andrews, R.M., Kubacka, I., Chinnery, P.F., Lightowlers, R.N., Turnbull, D.M., Howell, N., 1999. Reanalysis and revision of the Cambridge reference sequence for human mitochondrial DNA. *Nature Genetics* 23, 147.
- Arnaud, J., Peretto, C., Panetta, D., Tripodi, M., Fontana, F., Arzarello, M., Thun Hohenstein, U., Berto, C. Sala, B., Oxilia, G., Salvadori, P.A., Benazzi, S., 2016. A reexamination of the Middle Paleolithic human remains from Riparo Tagliente, Italy. *Quaternary International* 425, 437–44.
- Arnaud, J., Benazzi, S., Romandini, M., Livraghi, A., Panetta, D., Salvadori, P.A., Volpe, L., Peresani, M., 2017. A Neanderthal deciduous human molar with incipient carious infection from the Middle Palaeolithic De Nadale cave, Italy. *American Journal of Physical Anthropology* 162, 370–376.
- Badino, F., Pini, R., Ravazzi, C., Margaritora, D., Arrighi, S., Bortolini, E., Figus, C., Giaccio, B., Lugli, F., Marciani, G., Monegato, G., Moroni, A., Negrino, F., Oxilia, G., Peresani, M.,

This item was downloaded from IRIS Università di Bologna (<https://cris.unibo.it/>)

When citing, please refer to the published version.

- Romandini, M., Ronchitelli, A., Spinapolice, E.E., Zerboni, A., Benazzi S., 2019. An overview of Alpine and Mediterranean palaeogeography, terrestrial ecosystems and climate history during MIS 3 with focus on the Middle to Upper Palaeolithic transition. *Quaternary International*. <https://doi.org/10.1016/j.quaint.2019.09.024>.
- Bar-Yosef, O., 2003. Reflections on selected issues of the Upper Palaeolithic. In: Goring-Morris, A.N., Belfer-Cohen, A. (Eds.), *More than Meets the Eye. Studies on Upper Palaeolithic Diversity in the Near East*. Oxbow Books, Oxford, pp. 265-273.
- Bar-Yosef, O., 2007. The archaeological framework of the Upper Paleolithic revolution. *Diogenes* 214, 3-18.
- Bar-Matthews, M., Avalon, A., Kaufman, A., 2000. Timing and hydrological conditions of sapropel events in the Eastern Mediterranean as evident from speleothems, Soreq cave, Israel. *Chemical Geology* 169, 145-156.
- Becam, G., Chevalier, T., 2019. Neandertal features of the deciduous and permanent teeth from Portel-Ouest Cave (Ariège, France). *American Journal of Physical Anthropology* 168, 45-69.
- Been, E., Hovers, E., Ekshtain, R., Malinski-Buller, A., Agha, N., Barash, A., Bar-Yosef, O., Mayer, D.E., Benazzi, S., Hublin, J.-J., Levin, L., Greenbaum, N., Mitki, N., Oxilia, G., Porat, N., Roskin, J., Soudack, M., Yeshurun, R., Shahack-Gross, R., Nir, N., Stahlschmidt, M.C., Rak, Y., Barzilai, O., 2017. The first Neanderthal remains from an open-air Middle Palaeolithic site in the Levant. *Scientific Reports* 7, 2958.
- Benazzi, S., Douka, K., Fornai, C., Bauer, C. C., Kullmer, O., Svoboda, J., et al., 2011a. Early dispersal of modern humans in Europe and implications for Neanderthal behaviour. *Nature* 479, 525-528.

This item was downloaded from IRIS Università di Bologna (<https://cris.unibo.it/>)

When citing, please refer to the published version.

- Benazzi, S., Fornai, C., Bayle, P., Coquerelle, M., Kullmer, O., Mallegni, F., Weber, G.W., 2011b. Comparison of dental measurement systems for taxonomic assignment of Neanderthal and modern human lower second deciduous molars. *Journal of Human Evolution* 61, 320-326.
- Benazzi, S. 2012. The first modern Europeans. *Journal of Anthropological Sciences* 90, 3-6.
- Benazzi, S., Bailey, S.E., Mallegni, F., 2013. A morphometric analysis of the Neanderthal upper second molar Leuca I. *American Journal of Physical Anthropology* 152, 300-305.
- Benazzi, S., Panetta, D., Fornai, C., Toussaint, M., Gruppioni, G., Hublin, J.-J., 2014a. Guidelines for the digital computation of 2D and 3D enamel thickness. *American Journal of Physical Anthropology* 153, 305-313.
- Benazzi, S., Bailey, S.E., Peresani, M., Mannino, M.A., Romandini, M., Richards, M.P., Hublin, J. J., 2014b. Middle Paleolithic and Uluzzian human remains from Fumane Cave, Italy. *Journal of Human Evolution* 70, 61-68.
- Benazzi, S., Slon, V., Talamo, S., Negrino, F., Peresani, M., Bailey, S.E., Sawyer, S., Panetta, D., Vicino, G., Starnini, E., Mannino, M.A., Salvadori, P.A., Meyer, M., Pääbo, S., Hublin, J.-J., 2015. The makers of the protoaurignacian and implications for Neanderthal extinction. *Science* 348, 793-796.
- Bouckaert, R., Heled, J., Kühnert, D., Vaughan, T., Wu, C.-H., Xie, D., Suchard, M.A., Rambaut, A., Drummond, A.J., 2014. BEAST 2: a software platform for Bayesian evolutionary analysis. *PLoS Computational Biology* 10, e1003537.
- Briggs, A.W., Stenzel, U., Johnson, P.L., Green, R.E., Kelso, J., Prüfer, K., Meyer, M., Krause, J., Ronan, M.T., Lachmann, M., Pääbo, S., 2007. Patterns of damage in genomic DNA sequences from a Neandertal. *Proceedings of the National Academy of Sciences USA* 104, 14616-14621.
- Briggs, A.W., Good, J.M., Green, R.E., Krause, J., Maricic, T., Stenzel, U., Lalueza-Fox, C., Rudan, P., Brajkovic, D., Kucan, Z., Gusic, I., Schmitz, R., Doronichev, V.B., Golovanova, L.V., de la

This item was downloaded from IRIS Università di Bologna (<https://cris.unibo.it/>)

When citing, please refer to the published version.

- Rasilla, M., Fortea, J., Rosas, A., Pääbo, S., 2009. Targeted retrieval and analysis of five Neanderthal mtDNA genomes. *Science* 325, 318-321.
- Brock, F., Higham, T.F.G., Ditchfield, P & Bronk Ramsey, C., 2010. Current Pretreatment Methods for AMS Radiocarbon Dating at the Oxford Radiocarbon Accelerator Unit (ORAU). *Radiocarbon* 52, 103-112.
- Bronk Ramsey, C., 2009. Bayesian analysis of radiocarbon dates. *Radiocarbon* 51, 337-360.
- Brown, S., Higham, T., Slon, V., Pääbo, S., Meyer, M., Douka, K., Brock, F., Comeskey, D., Procopio, N., Shunkov, M., Derevianko A., Buckley, M., 2016. Identification of a new hominin bone from Denisova Cave, Siberia using collagen fingerprinting and mitochondrial DNA analysis. *Scientific Reports* 6, 23559.
- Brown, T.A, Nelson, D.E, Vogel, J.S, Southon, J.R., 1988. Improved collagen extraction by modified Longin method. *Radiocarbon* 30, 171-177.
- Buti, L., Le Cabec, A., Panetta, D., Tripodi, M., Salvadori, P.A., Hublin, J.-J., Feeney, R.N.M., Benazzi, S., 2017. 3D enamel thickness in Neanderthal and modern human permanent canines. *Journal of Human Evolution* 113, 162-172.
- Champely, S., 2018. pwr: Basic Functions for Power Analysis. R package version 1.2-2. <https://CRAN.R-project.org/package=pwr>.
- Charney, N., Record, S., 2012. vegetarian: Jost Diversity Measures for Community Data. R package version 1.2. <https://CRAN.R-project.org/package=vegetarian>.
- Dal Lago, A., Mietto, P., 2003. Grotte dei Berici. Aspetti Fisici e Naturalistici. Museo Naturalistico Archeologico, Vicenza.
- Darfeuil, S., Ménot, G., Giraud, X., Rostek, F., Tachikawa, K., Garcia, M., Bard, É., 2016. Sea surface temperature reconstructions over the last 70 kyr off Portugal: Biomarker data and regional modeling. *Paleoceanography* 31, 40-65.

This item was downloaded from IRIS Università di Bologna (<https://cris.unibo.it/>)

When citing, please refer to the published version.

- Dean, M.C. Wood, B., 2003. A digital radiographic atlas of great apes skull and dentition. In: Bondioli, L., Macchiarelli, R. (Eds.), Digital Archives of Human Paleobiology 3. Museo Nazionale Preistorico Etnografico Luigi Pigorini, Roma. Ermini, L., Olivieri, C., Rizzi, E., Corti, G., Bonnal, R., Soares, P., Luciani, S., Marota, I., De Bellis, G., Richards, M.B., Rollo, F., 2008. Complete mitochondrial genome sequence of the Tyrolean Iceman. *Current Biology* 18, 1687-1693.
- Fabbri, P.F., Panetta, D., Sarti, L., Martini, F., Salvadori, P.A., Caramella, D., Fedi, M., Benazzi, S., 2016. Middle paleolithic human deciduous incisor from Grotta del Cavallo, Italy. *American Journal of Physical Anthropology* 161, 506-512.
- Feldkamp, I.A., Davis, L.C., Kress, J.W., 1984. Practical cone-beam algorithm. *Journal of the Optical Society of America A-Optics and Image Science and Vision* 6, 612-619.
- Fewlass, H., Talamo, S., Wacker, L., Kromer, B., Tuna T., Fagault, Y., Bard, E., McPherron, S.P., Aldeias, V., Maria, R., Martisius, N.L., Paskulin, L., Rezek, Z., Sinet-Mathiot, V., Sirakova, S., Smith, G.M., Spasov, R., Welker, F., Sirakov, N., Tsanova T., Hublin, J.-J., 2020. A ¹⁴C chronology for the Middle to Upper Palaeolithic transition at Bacho Kiro Cave, Bulgaria. *Nature Ecology and Evolution* 4, 794–801.
- Fiorenza, L., Benazzi, S., Oxilia, G., Kullmer, O., 2018. Functional relationship between dental macrowear and diet in Late Pleistocene and recent modern human populations. *International Journal of Osteoarchaeology* 28, 153–161.
- Fleitmann, D., Cheng, H., Badertscher, S., Edwards, R.L., Mudelsee, M., Gökçürk, O.M., Fankhauser A., Pickering R., Raible C.C., Matter A, Kramers J, Tüysüz O., 2009. Timing and climatic impact of Greenland interstadials recorded in stalagmites from northern Turkey. *Geophysical Research Letters* 36, L19707.

This item was downloaded from IRIS Università di Bologna (<https://cris.unibo.it/>)

When citing, please refer to the published version.

- Fletcher, W., and Sánchez Goñi, M., 2008. Orbital- and sub-orbital-scale climate impacts on vegetation of the western Mediterranean basin over the last 48,000 yr. *Quaternary Research* 70, 451-464.
- Fletcher, W.J., Sánchez Goñi, M. F., Allen, J. R. M., Cheddadi, R., Comborieu-Nebout, N., Huntley, B., Lawson, I., Londeix, L., Magri, D., Margari, V., Müller, U. C., Naughton, F., Novenko, E., Roucoux, K., Tzedakis, P.C., 2010. Millennial scale variability during the last glacial in vegetation records from Europe. *Quaternary Science Reviews* 29, 2839-2864.
- Fu, Q., Meyer, M., Gao, X., Stenzel, U., Burbano, H.A., Kelso, J., Pääbo, S., 2013a. DNA analysis of an early modern human from Tianyuan Cave, China. *Proceedings of the National Academy of Sciences USA* 110, 2223-2227.
- Fu, Q., Mittnik, A., Johnson, P.L.F., Bos, K., Lari, M., Bollongino, R., Sun, C., Giemsch, L., Schmitz, R., Burger, J., Ronchitelli, A.M., Martini, F., Cremonesi, R.G., Svoboda, J., Bauer, P., Caramelli, D., Castellano, S., Reich, D., Pääbo, S., Krause, J., 2013b. A revised timescale for human evolution based on ancient mitochondrial genomes. *Current Biology* 23, 553-559.
- Fu, Q., Li, H., Moorjani, P., Jay, F., Slepchenko, S.M., Bondarev, A.A., Johnson, P.L., Aximu-Petri, A., Prüfer, K., de Filippo, C., Meyer, M., Zwyns, N., Salazar-García, D.C., Kuzmin, Y.V., Keates, S.G., Kosintsev, P.A., Razhev, D.I., Richards, M.P., Peristov, N.V., Lachmann, M., Douka, K., Higham, T.F., Slatkin, M., Hublin, J.-J., Reich, D., Kelso, J., Viola, T.B., Pääbo, S., 2014. Genome sequence of a 45,000-year-old modern human from western Siberia. *Nature* 514, 445-449.
- Gansauge, M.T., Meyer, M., 2013. Single-stranded DNA library preparation for the sequencing of ancient or damaged DNA. *Nature Protocol* 8, 737-748.
- Gansauge, M.T., Meyer, M., 2014. Selective enrichment of damaged DNA molecules for ancient genome sequencing. *Genome Research* 24, 1543-1549.

This item was downloaded from IRIS Università di Bologna (<https://cris.unibo.it/>)

When citing, please refer to the published version.

- Gansauge, M.T., Gerber, T., Glocke, I., Korlevic, P., Lippik, L., Nagel, S., Riehl, L.M., Schmidt, A., Meyer, M., 2017. Single-stranded DNA library preparation from highly degraded DNA using T4 DNA ligase. *Nucleic Acids Research* 45, 79.
- Gargett, R.H., 1989. The evidence for Neandertal burial. *Current Anthropology* 30, 157-190.
- Garralda, M.D., Galván, B., Hernández, C. M., Mallol, C., Gómez, J. A, Maureille, B., 2014. Neanderthals from El Salt (Alcoy, Spain) in the context of the latest Middle Palaeolithic populations from the southeast of the Iberian Peninsula. *Journal of Human Evolution* 75, 1-15.
- Gilbert, M.T., Kivisild, T., Grønnow, B., Andersen, P.K., Metspalu, E., Reidla, M., Tamm, E., Axelsson, E., Götherström, A., Campos, P.F., Rasmussen, M., Metspalu, M., Higham, T.F., Schwenninger, J.L., Nathan, R., De Hoog, C.J., Koch, A., Møller, L.N., Andreasen, C., Meldgaard, M., Villem, R., Bendixen, C., Willerslev, E., 2008. Paleo-Eskimo mtDNA genome reveals matrilineal discontinuity in Greenland. *Science* 320, 1787-1789.
- Glocke, I., Meyer, M., 2017. Extending the spectrum of DNA sequences retrieved from ancient bones and teeth. *Genome Research* 27, 1230-1237.
- Green, R.E., Malaspina, A.S., Krause, J., Briggs, A.W., Johnson, P.L., Uhler, C., Meyer, M., Good, J.M., Maricic, T., Stenzel, U., Prüfer, K., Siebauer, M., Burbano, H.A., Ronan, M., Rothberg, J.M., Egholm, M., Rudan, P., Brajković, D., Kućan, Z., Gusić, I., Wikström, M., Laakkonen, L., Kelso, J., Slatkin, M., Pääbo, S., 2008. A complete Neanderthal mitochondrial genome sequence determined by high-throughput sequencing. *Cell* 134, 416-426.
- Gómez-Olivencia, A., Rolf, Q., Sala, N., Bardey, M., Ohman, J.C., Antoine, B., 2018. La Ferrassie 1: new perspectives on a 'classic' Neanderthal. *Journal of Human Evolution* 117, 13-32.
- Guerin, G., Frouin, M., Talamo, S., Aldeias, V., Bruxelles, L., Chiotti, L., Dibble, H.L., Goldberg, P., Hublin, J.-J., Jain, M., Lahaye, C., Madelaine, S., Maureille, B., McPherron, S.J.P., Mercier, N., Murray, A.S., Sandgathe, D., Steele, T.E., Thomsen, K.J., Turq, A., 2015. A multi-method

This item was downloaded from IRIS Università di Bologna (<https://cris.unibo.it/>)

When citing, please refer to the published version.

luminescence dating of the Palaeolithic sequence of La Ferrassie based on new excavations adjacent to the La Ferrassie 1 and 2 skeletons. *Journal of Archaeological Science* 58, 147-166.

Hajdinjak, M., Fu, Q., Hübner, A., Petr, M., Mafessoni, F., Grote, S., Skoglund, P., Narasimham, V., Rougier, H., Crevecoeur, I., Semal, P., Soressi, M., Talamo, S., Hublin, J.-J., Gušić, I., Kućan, Ž., Rudan, P., Golovanova, L.V., Doronichev, V.B., Posth, C., Krause, J., Korlević, P., Nagel, S., Nickel, B., Slatkin, M., Patterson, N., Reich, D., Prüfer, K., Meyer, M., Pääbo S., Kelso, J., 2018. Reconstructing the genetic history of late Neanderthals. *Nature* 555, 652-656.

Harvati, K., Panagopoulou, E., Karkanas, P., 2003. First Neanderthal remains from Greece: the evidence from Lakonis. *Journal of Human Evolution* 45, 465-473.

Higham, T., Douka, K., Wood, R., Bronk Ramsey, C., Brock, F., Basell, L., Camps, M., Arrizabalaga, A., Baena, J., Barroso-Ruíz, C., Bergman, C., Boitard, C., Boscato, P., Caparrós, M., Conard, N.J., Driaily, C., Froment, A., Galván, B., Gambassini, P., Garcia-Moreno, A., Grimaldi, S., Haesaerts, P., Holt, B., Iriarte-Chiapusso, M.J., Jelinek, A., Jordá Pardo, J.F., Maíllo-Fernández, J.M., Marom, A., Maroto, J., Menéndez, M., Metz, L., Morin, E., Moroni, A., Negrino, F., Panagopoulou, E., Peresani, M., Pirson, S., de la Rasilla, M., Riel-Salvatore, J., Ronchitelli, A., Santamaria, D., Semal, P., Slimak, L., Soler, J., Soler, N., Villaluenga, A., Pinhasi, R., Jacobi, R., 2014. The timing and spatio-temporal patterning of Neanderthal disappearance. *Nature* 512, 306-309.

Higham, T.F.G., Jacobi, R.M., Bronk Ramsey, C., 2006. AMS radiocarbon dating of ancient bone using ultrafiltration. *Radiocarbon* 48, 179-195.

Hoffecker, J.F., 2009. The spread of modern humans in Europe. *Proceedings of the National Academy of Sciences USA* 106, 16040-16045.

Hublin, J.-J., 2015. The modern human colonization of western Eurasia: when and where? *Quaternary Science Reviews* 118, 194-210.

This item was downloaded from IRIS Università di Bologna (<https://cris.unibo.it/>)

When citing, please refer to the published version.

- Hublin, J.-J., Sirakov, N., Aldeias, V., Bailey, S., Bard, E., Delvigne V., Endarova, E., Fagault, Y., Fewlass, H., Hajdinjak, M., Kromer, B., Krumov, I., Marreiros, J., Martisius, N.L., Paskulin P., Sinet-Mathiot, V., Meyer, M., Pääbo, S., Popov, V., Rezek, Z., Sirakova, S., Skinner, M.-M., Geoff M. Smith, G.M., Spasov, R., Talamo, S., Tuna, T., Wacker, L., Welker, F., Wilcke, A., Zahariev, N., McPherron, S.P., Tsanova, T., 2020. Initial Upper Palaeolithic *Homo sapiens* from Bacho Kiro Cave, Bulgaria. *Nature* 581, 299–302.
- Ingman, M., Kaessmann, H., Pääbo, S., Gyllensten, U., 2000. Mitochondrial genome variation and the origin of modern humans. *Nature* 408, 708-713.
- Jelinek, J., 1980. Neanderthal Remains in Kůlna Cave, Czechoslovakia. In: Schwidetzky, I., Chiarelli, B., Necrasov, O. (Eds.), *Physical Anthropology of European Populations*. Mouton, The Hague, pp. 351–353.
- Jost, L., 2007. Partitioning diversity into independent alpha and beta components. *Ecology* 88, 2427-2439.
- Kircher, M., Sawyer, S., Meyer, M., 2012. Double indexing overcomes inaccuracies in multiplex sequencing on the Illumina platform. *Nucleic Acids Research* 40, 3.
- Krause, J., Krause, J., Fu, Q., Good, J.M., Viola, B., Shunkov, M.V., Derevianko, A.P., Pääbo, S., 2010a. The complete mitochondrial DNA genome of an unknown hominin from southern Siberia. *Nature* 464, 894-897.
- Krause, J., Briggs, A.W., Kircher, M., Maricic, T., Zwyns, N., Derevianko, A., Pääbo, S., 2010b. A complete mtDNA genome of an early modern human from Kostenki, Russia. *Current Biology* 20, 231-236.
- Le Luyer, M., Rottier, S., Bayle, P., 2014. Brief communication: comparative patterns of enamel thickness topography and oblique molar wear in two Early Neolithic and medieval population samples. *American Journal of Physical Anthropology* 155, 162–172.

This item was downloaded from IRIS Università di Bologna (<https://cris.unibo.it/>)

When citing, please refer to the published version.

- Livraghi, A., Fanfarillo, G., Dal Colle, M., Romandini, M., Peresani, M., 2019. Neanderthal ecology and exploitation of cervids at the onset of MIS4: A study on De Nadale cave, Italy. *Quaternary International*. <https://doi.org/10.1016/j.quaint.2019.11.024>
- López-García, JM, Dalla Valle, C., Cremaschi, M., Peresani, M., 2015. Reconstruction of the Neanderthal and modern human landscape and climate from the Fumane cave sequence (Verona, Italy) using small-mammal assemblages. *Quaternary Science Reviews* 128, 1–13.
- López-García, J.M., Berto, C., Peresani, M., 2019. Environmental and climatic context of the hominin occurrence in northeastern Italy from the late Middle to Late Pleistocene inferred from small-mammal assemblages. *Quaternary Science Reviews* 216, 18-33.
- Macchiarelli, R., Mazurier, A., Volpato, V., 2007. L'apport des nouvelles technologies à l'étude des Néandertaliens. In: Vandermeersch B., Maureille B. (Eds.), *Les Néandertaliens, Biologie et Cultures*. CTHS, Paris, pp. 169-179.
- Madrigal, L. (Ed.), 2012. *Statistics for Anthropology*, 2nd ed. Cambridge University Press, New York.
- Maricic, T., Whitten, M., Pääbo, S., 2010. Multiplexed DNA sequence capture of mitochondrial genomes using PCR products. *PLoS One* 5, e14004.
- Margherita, C., Oxilia, G., Barbi, V., Panetta, D., Hublin, J.-J., Lordkipanidze, D., Meshveliani, T., Jakeli, N., Matskevich, Z., Bar-Yosef, O., Belfer-Cohen, A., Pinhasi, R., Benazzi, S., 2017. Morphological description and morphometric analyses of the Upper Palaeolithic human remains from Dzudzuana and Satsurbliia caves, western Georgia. *Journal of Human Evolution* 113, 83–90.
- Margherita, C., Talamo, S., Wiltschke-Schrotta, K., Senck, S., Oxilia, G., Sorrentino, R., Mancuso, G., Gruppioni, G., Lindner, R., Hublin, J.-J., Benazzi, S., 2016. A reassessment of the presumed Torrener Bärenhöhle's Paleolithic human tooth. *Journal of Human Evolution* 93, 120–5.

This item was downloaded from IRIS Università di Bologna (<https://cris.unibo.it/>)

When citing, please refer to the published version.

- Meyer, M., Kircher, M., Gansauge, M.T., Li, H., Racimo, F., Mallick, S., Schraiber, J.G., Jay, F., Prüfer, K., de Filippo, C., Sudmant, P.H., Alkan, C., Fu, Q., Do, R., Rohland, N., Tandon, A., Siebauer, M., Green, R.E., Bryc, K., Briggs, A.W., Stenzel, U., Dabney, J., Shendure, J., Kitzman, J., Hammer, M.F., Shunkov, M.V., Derevianko, A.P., Patterson, N., Andrés, A.M., Eichler, E.E., Slatkin, M., Reich, D., Kelso, J., Pääbo, S., 2012. A high-coverage genome sequence from an archaic Denisovan individual. *Science* 338, 222-226.
- Meyer, M., Fu, Q., Aximu-Petri, A., Glocke, I., Nickel, B., Arsuaga, J.-L., Martínez, I., Gracia, A., Bermúdez de Castro, J.M., Carbonell, E., Pääbo, S., 2014. A mitochondrial genome sequence of a hominin from Sima de los Huesos. *Nature* 505, 403-406.
- Molnar, S., 1971. Human tooth wear, tooth function and cultural variability. *American Journal of Physical Anthropology* 34, 175-189.
- Moorrees, C.F., Fanning, E.A., Hunt, E.E., 1963. Formation and resorption of three deciduous teeth in children. *American Journal of Physical Anthropology* 21, 205-213.
- Moroni, A., Ronchitelli, A., Arrighi, S., Aureli, D., Bailey, S., Boscato, P., Boschin, F., Capecchi, G., Crezzini, J., Douka, K., Marciani, G., Panetta, D., Ranaldo, F., Ricci, S., Scaramucci, S., Spagnolo, V., Benazzi, S., Gambassini, P., 2018. Grotta del Cavallo (Apulia – Southern Italy). The Uluzzian in the mirror. *Journal of Anthropological Sciences* 96, 1-36.
- Müller, U.C., Pross, J., Tzedakis, P.C., Gamble, C., Kotthoff, U., Schmiedl, G., Wulf, S., Christanis, K., 2011. The role of climate in the spread of modern humans into Europe. *Quaternary Science Reviews* 30, 273-279.
- Panetta, D., Belcari, N., Del Guerra, A., Bartolomei, A., Salvadori, P.A., 2012. Analysis of image sharpness reproducibility on a novel engineered micro-CT scanner with variable geometry and embedded recalibration software. *Physica Medica* 28, 166-173.

This item was downloaded from IRIS Università di Bologna (<https://cris.unibo.it/>)

When citing, please refer to the published version.

- Peresani, M., 2008. A new cultural frontier for the last Neanderthals: the Uluzzian in Northern Italy. *Current Anthropology* 49, 725-731.
- Peresani, M., 2011. The end of the Middle Palaeolithic in the Italian Alps. An overview on Neanderthal land-use, subsistence and technology. In: Conrads, N. and Richter, J. (Eds.), *Neanderthal Lifeways, Subsistence and Technology. One Hundred Fifty Years of Neanderthal Study*. Springer, Dordrecht, pp. 249-259.
- Peresani, M., Cristiani, E., Romandini, M., 2016, The Uluzzian technology of Grotta di Fumane and its implication for reconstructing cultural dynamics in the Middle – Upper Palaeolithic transition of Western Eurasia. *Journal of Human Evolution* 91, 36-56.
- Peresani, M., Bertola, S., Delpiano, D., Benazzi, S., Romandini, M., 2019. The Uluzzian in the north of Italy: insights around the new evidence at Riparo Broion. *Archaeological and Anthropological Sciences* 11, 3503-3536.
- Peretto, C., Biagi, P., Boschian, G., Broglio, A., de Stefani, M., Fasani, L., Fontana, F., Grifoni, R., Guerreschi, A., Iacopini, A., Minelli, A., Pala, F., Peresani, M., Radi, G., Ronchitelli, A., Sarti, L., Thun-Hohenstein, U., Tozzi, C., 2004. Living-Floors and Structures from the Lower Palaeolithic to the Bronze Age. In: Facchini, F., Belcastro, A., Thun-Hohenstein, U. (Eds.), *Evolution of the Human Peopling in Italy-Paleobiology, Behavior, Subsistence Strategies. A Research Program Financed by the MIUR (Ministry of Education, University and Research), Collegium Antropologicum* 28,63-88.
- Peyrégne, S., Slon, V., Mafessoni, F., de Filippo, C., Hajdinjak, M., Nagel, S., Nickel, B., Essel, E., Le Cabec, A., Wehrberger, K., Conard, N.J., Kind, C.J., Posth, C., Krause, J., Abrams, G., Bonjean, D., Di Modica, K., Toussaint, M., Kelso., J., Meyer, M., Pääbo, S., Prüfer, K., 2019. Nuclear DNA from two early Neanderthals reveals 80,000 years of genetic continuity in Europe. *Science Advances* 5, eaaw5873.

This item was downloaded from IRIS Università di Bologna (<https://cris.unibo.it/>)

When citing, please refer to the published version.

- Pini, R., Ravazzi, C., Donegana, M., 2009. Pollen stratigraphy, vegetation and climate history of the last 215 ka in the Azzano Decimo core (plain of Friuli, north-eastern Italy). *Quaternary Science Reviews* 28, 1268-1290.
- Pini, R., Ravazzi, C., Reimer P.J., 2010. The vegetation and climate history of the last glacial cycle in a new pollen record from Lake Fimon (southern Alpine foreland, N-Italy). *Quaternary Science Reviews* 29, 3115-3137.
- Prentice, I. C., Cramer, W., Harrison, S. P., Leemans, R., Monserud, R. A., Solomon, A.M., 1992. Special paper: a global biome model based on plant physiology and dominance, soil properties and climate. *Journal of Biogeography* 19, 117-134.
- Prüfer, K., Racimo, F., Patterson, N., Jay, F., Sankararaman, S., Sawyer, S., Heinze, A., Renaud, G., Sudmant, P.H., de Filippo, C., Li, H., Mallick, S., Dannemann, M., Fu, Q., Kircher, M., Kuhlwilm, M., Lachmann, M., Meyer, M., Ongyerth, M., Siebauer, M., Theunert, C., Tandon, A., Moorjani, P., Pickrell, J., Mullikin, J.C., Vohr, S.H., Green, R.E., Hellmann, I., Johnson, P.L.F., Blanche, H., Cann, H., Kitzman, J.O., Shendure, J., Eichler, E.E., Lein, E.S., Bakken, T.E., Golovanova, L.V., Doronichev, V.B., Shunkov, M.V., Derevianko, A.P., Viola, B., Slatkin, M., Reich, D., Kelso, J., Pääbo, S., 2014. The complete genome sequence of a Neanderthal from the Altai Mountains. *Nature* 505, 43-49.
- Rasmussen, S.O., Bigler, M., Blockley, S.P., Blunier, T., Buchardt, S.L., Clausen, H.B., Cvijanovic, I., Dahl-Jensen, D., Johnsen, S.J., Fischer, H., 2014. A stratigraphic framework for abrupt climatic changes during the Last Glacial period based on three synchronized Greenland ice-core records: refining and extending the INTIMATE event stratigraphy. *Quaternary Science Reviews* 106, 14-28.
- R Core Team, 2018. R: A language and environment for statistical computing. R Foundation for Statistical Computing, Vienna.

This item was downloaded from IRIS Università di Bologna (<https://cris.unibo.it/>)

When citing, please refer to the published version.

- Reich, D., Green, R.E., Kircher, M., Krause, J., Patterson, N., Durand, E.Y., Viola, B., Briggs, A.W., Stenzel, U., Johnson, P.L., Maricic, T., Good, J.M., Marques-Bonet, T., Alkan, C., Fu, Q., Mallick, S., Li, H., Meyer, M., Eichler, E.E., Stoneking, M., Richards, M., Talamo, S., Shunkov, M.V., Derevianko, A.P., Hublin, J.J., Kelso, J., Slatkin, M., Paabo, S., 2010. Genetic history of an archaic hominin group from Denisova Cave in Siberia. *Nature* 468, 1053-1060.
- Reimer, P.J., Bard, E., Bayliss, A., Beck, J.W., Blackwell, P.G., Bronk Ramsey, C., Grootes, P.M., Guilderson, T.P., Hafliðason, H., Hajdas, I., Hatté, C., Heaton, T.J., Hoffmann, D.L., Hogg, A.G., Hughen, K.A., Kaiser, K.F., Kromer, B., Manning, S.W., Mu Niu, Reimer, R.W., Richards, D.A., Scott, E.M., Southon, J.R., Staff, R.A., Turney, C.S.M., Van der Plicht, J., 2013. IntCal13 and Marine13 radiocarbon age calibration curves 0–50,000 years cal BP. *Radiocarbon* 55, 1869-1887.
- Richter, D., Tostevin, G., Skrdla, P., Davies, W., 2009. New radiometric ages for the early Upper Palaeolithic type locality of Brno-Bohunice (Czech Republic): comparison of OSL, IRSL, TL and ¹⁴C dating results. *Journal of Archaeological Science* 36, 708-720.
- Rohland, N., Glocke, I., Aximu-Petri, A., Meyer, M., 2018. Extraction of highly degraded DNA from ancient bones, teeth and sediments for high-throughput sequencing. *Nature Protocols* 13, 2447-2461.
- Romandini, M., Nannini, N., Tagliacozzo, A., Peresani, M., 2014. The ungulate assemblage from layer A9 at Grotta di Fumane, Italy: a zooarchaeological contribution to the reconstruction of Neanderthal ecology. *Quaternary International* 337, 11-27.
- Romandini, M., Crezzini, J., Bortolini, E., Boscato, P., Boschini, F., Carrera, L., Nannini, N., Tagliacozzo, A., Terlato, G., Arrighi, S., Badino, F., Figus, C., Lugli, F., Marciani, G., Oxilia, G., Moroni, A., Negrino, F., Marco, P., Riel-Salvatore, J., Ronchitelli, A., Spinapolice, E.E., Benazzi S., 2019. Macromammal and bird assemblages across the Late Middle to Upper Palaeolithic

This item was downloaded from IRIS Università di Bologna (<https://cris.unibo.it/>)

When citing, please refer to the published version.

transition in Italy: an extended zooarchaeological review. *Quaternary International*.
<https://doi.org/10.1016/j.quaint.2019.11.008>.

Rosas, A., Ríos, L., Estalrich, A., Liversidge, H., García-Taberner, A., Huguet, R., Cardoso, H., Bastir, M., Lalueza-Fox, C., de la Rasilla, M., Dean, C., 2017. The growth pattern of Neandertals, reconstructed from a juvenile skeleton from El Sidrón (Spain). *Science* 22, 1282-1287.

Rougier, H., Crevecoeur, I., Beauval, C., Posth, C., Flas, D., Wißing, C., Furtwängler, A., Germonpré, M., Gómez-Olivencia, A., Semal, P., van der Plicht, J., Bocherens, H., Krause, J., 2016. Neanderthal cannibalism and Neanderthal bones used as tools in Northern Europe. *Scientific Reports* 6, 29005.

Ruiz, C. B., Caparrós, M., Barsky, D., Moigne, A. M., Bohórquez, A. M., 2014. Boquete de Zafarraya cave: a Neanderthal site in southern Iberia. In: Ramos, R.S., Carbonell, E.J.M., de Castro, B., Arsuaga, J.L. (Eds), *Pleistocene and Holocene Hunter-Gatherers in Iberia and the Gibraltar Strait: The Current Archaeological Record*. Fundación Atapuerca, Burgos, pp. 463-472.

Sauro, U., 2002. The Monti Berici: A peculiar type of karst in the southern Alps. *Acta Carsologica* 31(3), 99-114.

Sawyer, S., Renaud, G., Viola, B., Hublin, J.-J., Gansauge, M.-T., Shunkov, M.V., Derevianko, A.P., Prüfer, K., Kelso, J., Pääbo, S., 2015. Nuclear and mitochondrial DNA sequences from two Denisovan individuals. *Proceedings of the National Academy of Sciences USA* 112, 15696-15700.

Skoglund, P., Northoff, B.H., Shunkov, M.V., Derevianko, A.P., Pääbo, S., Krause, J., Jakobsson, M., 2014. Separating endogenous ancient DNA from modern day contamination in a Siberian Neanderthal. *Proceedings of the National Academy of Sciences USA* 111, 2229-2234.

Semal, P., Rougier, H., Crevecoeur, I., Jungels, C., Flas, D., Hauzeur, A., Maureille, B., Germonpre', M., Bocherens, H., Pirson, S., Cammaert, L., De Clerck, N., Hambucken, A., Higham, T.,

This item was downloaded from IRIS Università di Bologna (<https://cris.unibo.it/>)

When citing, please refer to the published version.

- Toussaint, M., Van der Plicht, J, 2009. New Data on the Late Neandertals: Direct Dating of the Belgian Spy Fossils, *American Journal of Physical Anthropology* 138, 421–428.
- Skrdla, P., 2003. Comparison of Boker Tachtit and Stranska skala MP/UP transitional industries. *Journal of the Israel Prehistoric Society* 33, 37-73.
- Slon, V., Viola, B., Renaud, G., Gansauge, M.-T., Benazzi, S., Sawyer, S., Hublin, J.-J., Shunkov, M.V., Derevianko, A.P., Kelso, J., Prüfer, K., Meyer, M., Pääbo, S., 2017. A fourth Denisovan individual. *Science Advances* 3, e1700186.
- Sokal, R.R., Rohlf, F.J. (Eds.), 1995. *Biometry. The Principles and Practice of Statistics in Biological Research*, 3rd ed. Freeman and Company Ltd, New York.
- Stuiver, M. and Polach, H. A., 1977. Discussion: Reporting of ¹⁴C Data. *Radiocarbon* 19, 355-363.
- Tillier A. M., 1982. Les enfants néandertaliens de Devils Tower (Gibraltar). *Z. Morph. Anthropol.*, 73, 125–148.
- Torchiano, M., 2018. *effsize: Efficient Effect Size Computation*. R package version 0.7.4. <https://CRAN.R-project.org/package=effsize>.
- Tostevin, G.B., 2003. A quest for antecedents: a comparison of the terminal Middle Palaeolithic and early Upper Palaeolithic of the Levant. In: Goring-Morris, A.N., Belfer-Cohen, A. (Eds.), *More than Meets the Eye. Studies on Upper Palaeolithic Diversity in the Near East*. Oxbow Books, Oxford, pp. 54-67.
- Turner, C.G., Nichol, C.R., Scott, G.R., 1991. Scoring procedures for key morphological traits of the permanent dentition: the Arizona State University dental anthropology system. In: Kelley, M.A., Larsen, C.S. (Eds.), *Advances in Dental Anthropology*. Wiley-Liss, New York, pp. 13-31.
- Tzedakis, P.C., Hooghiemstra, H., Pälike, H., 2006. The last 1.35 million years at Tenaghi Philippon: revised chronostratigraphy and long-term vegetation trends. *Quaternary Science Reviews* 25, 3416-3430.

This item was downloaded from IRIS Università di Bologna (<https://cris.unibo.it/>)

When citing, please refer to the published version.

- Wood, R.E., Bronk Ramsey, C., Higham, T.F.G., 2010. Refining the ultrafiltration bone pretreatment background for radiocarbon dating at ORAU. *Radiocarbon* 52, 600–611.
- Weber, M., Scholz, D., Schröder-Ritzrau, A., Deininger, M., Spötl, C., Lugli, F., Mertz-Kraus, R., Jochum, K.P., Fohlmeister, J., Stumpf, C.F., Riechelmann, D.F.C., 2018. Evidence of warm and humid interstadials in central Europe during early MIS 3 revealed by a multi-proxy speleothem record. *Quaternary Science Reviews* 200, 276-286.
- Walker, M. J., Gibert, J., López, M. V., Lombardi, A. V., Pérez-Pérez, A., Zapata, J., Ortega, J., Higham, T., Pike, A., Schwenninger, J.-L., Zilhão, J., Trinkaus, E., 2008. Late Neandertals in Southeastern Iberia: Sima de las Palomas del Cabezo Gordo, Murcia, Spain. *Proceedings of the National Academy of Sciences USA* 105, 20631-20636.
- Wolpoff, M. H., Smith, F. H., Malez, M., Radovčić, J., Rukavina, D., 1981. Upper Pleistocene Remains from Vindija Cave, Croatia, Yugoslavia. *American Journal of Physical Anthropology* 54, 499–545.
- Zanchetta, G., Giaccio, B., Bini, M., Sarti, L., 2018. Tephrostratigraphy of Grotta del Cavallo, Southern Italy: insights on the chronology of Middle to Upper Palaeolithic transition in the Mediterranean. *Quaternary Science Reviews* 182, 65-77.
- Zollikofer, C. P., de León, M. S. P., Vandermeersch, B., Lévêque, F., 2002. Evidence for interpersonal violence in the St. Césaire Neanderthal. *Proceedings of the National Academy of Sciences USA* 99, 6444-6448.

This item was downloaded from IRIS Università di Bologna (<https://cris.unibo.it/>)

When citing, please refer to the published version.

This item was downloaded from IRIS Università di Bologna (<https://cris.unibo.it/>)

When citing, please refer to the published version.